Seismic investigations of the O'Higgins Seamount Group and Juan Fernández Ridge: Aseismic ridge emplacement and lithosphere hydration

H. Kopp, E. R. Flueh, C. Papenberg, and D. Klaeschen

IFM-GEOMAR, Leibniz-Institute for Marine Sciences, Kiel, Germany

Received 7 October 2003; revised 5 January 2004; accepted 17 January 2004; published 20 March 2004.

[1] The O'Higgins Seamount Group is a cluster of volcanic domes located 120 km west of the central Chilean Trench on the crest of the Juan Fernández Ridge. This aseismic hot spot track is subducting under South America triggering a belt of intraslab earthquake hypocenters extending about 700 km inland. The Juan Fernández Ridge marks the southern boundary of a shallow subduction segment. Subduction of oceanic basement relief has been suggested as a cause for the "flat" slab segments characterizing the Andean trench system. The Juan Fernández Ridge, however, shows only moderate crustal thickening, inadequate to cause significant buoyancy. In 2001, wide-angle seismic data were collected along two perpendicular profiles crossing the O'Higgins Group. We present tomographic images of the volcanic edifices and adjacent outer rise-trench environment, which indicate a magmatic origin of the seamounts dominated by extrusive processes. High-resolution bathymetric data yield a detailed image of a network of syngenetic structures reactivated in the outer rise setting. A pervasive fault pattern restricted to the hot spot modified lithosphere coincides with anomalous low upper mantle velocities gained from a tomographic inversion of seismic mantle phases. Reduced uppermost mantle velocities are solely found underneath the Juan Fernández Ridge and may indicate mineral alterations. Enhanced buoyancy due to crustal and upper mantle hydration may contribute an additional mechanism for shallow subduction, which prevails to the north after the southward migration of the Juan Fernández Ridge. *INDEX TERMS:* 8010 Structural Geology: Fractures and faults; 8015 Structural Geology: Local crustal structure; 8105 Tectonophysics: Continental margins and sedimentary basins (1212); 8180 Tectonophysics: Tomography; 8414 Volcanology: Eruption mechanisms; *KEYWORDS:* seismic tomography, mantle hydration, aseismic ridge, central Chilean margin, hot spot emplacement. **Citation:** Kopp, H., E. R. Flueh, C. Papenberg, and D. Klaeschen (2004), Seismic investigations of the O'Higgins Seamount Group and Juan Fernández Ridge: Aseismic ridge emplacement and lithosphere hydration, *Tectonics*, *23*, TC2009, doi:10.1029/2003TC001590.

0278-7407/04/2003TC001590

1. Introduction

[2] Subduction under South America is characterized by the variation in dip angle of the downgoing plate along the Andes, resulting in a segmentation of the margin [e.g., *Barazangi and Isacks*, 1976; *Cahill and Isacks*, 1992]. Segments of shallow subduction underneath Peru and central Chile (Figure 1) correlate with the absence of Quaternary volcanism and a central valley on the overriding plate. A causative relationship between the subduction of ocean floor morphology and the "flat slab" segments has been proposed [e.g., *Nur and Ben-Avraham*, 1981; *Pilger*, 1981] as most segment boundaries coincide with major bathymetric elevations on the oceanic plate. Offshore Valparaiso, Chile, the subduction of the hot spot-generated aseismic Juan Fernández Ridge correlates with a pronounced embayment in the shore line and a block in the axial transport of trench fill [*von Huene et al.*, 1997]. To the south of the ridge's entrance point, a shallow and sediment flooded trench concurs with accretionary processes, while a starved and deepening trench to the north of the barrier marks the transition to a non-accreting/erosive regime and flat slab subduction. The spatial correlation between the Juan Fernández Ridge and the southern segment boundary of the Chilean flat slab suggests a linkage between enhanced buoyancy of anomalous crust often found at aseismic ridges [e.g., *Grevemeyer et al.*, 2001; *Walther*, 2003] and the shallowing of the Wadati-Benioff zone here. Seismic investigations off Valparaiso [*Flueh et al.*, 1998] indicated only minor crustal thickening near the O'Higgins Seamount Group, inadequate to explain the extent of the flat slab to more than 700 km inland [*van Hunen et al.*, 2002]. In 2001, the SPOC project set out to further investigate the effects of subducting aseismic ridges on the seismicity and structure of the Chilean margin. We collected seismic wide-angle and swath bathymetric data to investigate the evolution mechanisms of the Juan Fernández Ridge and the impact of the modified oceanic crustal structure on the subduction processes. The seismic data indicate an extrusive origin for the volcanoes dotted along the Juan Fernández Ridge. Swath mapping shows that the incoming oceanic plate experiences bend-faulting in the outer rise setting, which however only across the Juan Fernández Ridge develops

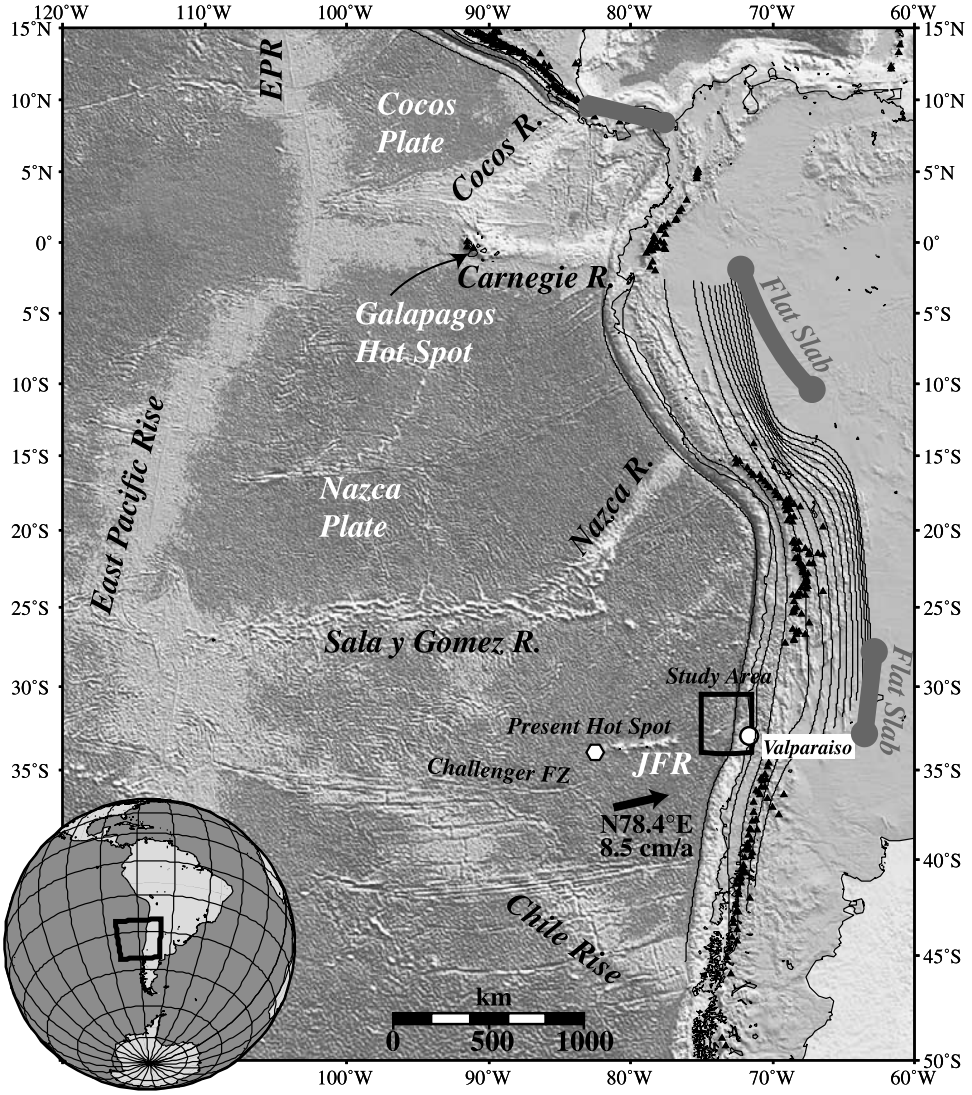

Figure 1. Geodynamic setting of the Nazca Plate. A number of hot spot generated aseismic ridges are currently being subducted along the Central and South American trench systems. A causative relationship between the subduction of bathymetric highs and the flat slab zones of shallow subduction may originate from buoyancy effects of anomalous thickened crust. The Juan Fernández Ridge (JFR) at the southern termination of the central Chile flat slab is of much smaller dimensions and does not show significant crustal thickening in the study area (shown by the black box). The Valparaiso embayment marks the collision point of the JFR with the Chilean shoreline. Black lines indicate Wadati-Benioff contours at 50 km intervals [*Gudmundsson and Sambridge*, 1998]. Volcanic activity (black triangles) is absent along the flat slab segments (taken from the Smithsonian Institution catalogue, available at http://www.volcano.si.edu/world/summinfo.cfm). Relative plate motion indicated by arrow [*DeMets et al.*, 1990].

into a pervasive tectonic fabric. Reactivation of inherited weak zones results in a deeply-penetrating fault pattern across the ridge. This pervasively faulted region is characterized by reduced upper mantle velocities (as low as 7.3 km s^{-1}) indicative of slab hydration and mineral alteration. Dehydration processes of the subducting lithosphere have been linked to intermediate-depth seismicity [*Kirby et al.*, 1996; *Peacock*, 2001; *Tibi et al.*, 2002; *Hacker et al.*, 2003b] and petrology alteration of the mantle wedge leading to partial melting [*Peacock*, 1990, 1993; *Bostock et al.*, 2002]. The locus of crust and mantle hydration remains debated, however [*Peacock*, 1990; *Seno and Yamanaka*, 1996; *Kirby et al.*, 1996; *Jiao et al.*, 2000; *Peacock*, 2001; *Ranero et al.*, 2003]. The results of this study indicate crust and uppermost mantle hydration to occur across the pervasively faulted outer rise region of the Juan Fernández Ridge. In contrast, the less developed fault patterns to the north and south of the ridge, which affect a

much smaller area of the incoming plate as the faulting commences closer to the trench, do not seem to promote sufficient hydration to be resolved by the seismic data.

2. Regional Tectonic Setting

[3] The O'Higgins Seamount Group, with O'Higgins Guyot and O'Higgins Seamount forming its two most prominent volcanic domes, is located 120 km west of the Chilean Trench (Figure 2), where Nazca plate subduction is occurring at a trend of 78.4° and a high convergence rate of 85 mm yr^{-1} [*DeMets et al.*, 1990, 1994] under the South American plate. The obliquely extending Challenger Fracture Zone, found offshore central Chile between 30°S and 35°S, delineates the Nazca plate into a southern domain, which forms at the Chile Rise, and a northern part originating at the Pacific-Nazca spreading center (Figure 1) [*Cande and Haxby*, 1991].

[4] Seafloor mapping based on satellite altimetry [*Sandwell and Smith*, 1997] reveals a 900 km long chain of 11 seamount groups that extend from the present hot spot at 97.5°W/34°S in an approximately W-E direction to the O'Higgins Group. The hot spot hypothesis for the aseismic Juan Fernández Ridge is supported by the linear increase in age along the chain as inferred from magnetic data [*Yáñez et al.*, 2001]. The chain appears as a continuous ridge west of 76.5°W. This segment of the ridge shows a free air gravity response characteristic of flexural loading of the oceanic crust [*Sandwell and Smith*, 1997]: a positive anomaly across the crest of the ridge is bordered by negative anomalies along both flanks, which indicate a moat structure. To the east, only isolated bathymetric elevations originating from episodic volcanic activity mark the plate's motion over the hot spot. As the Juan Fernández Ridge was not formed in proximity of a spreading ridge, it is of modest dimensions (Figure 1), unlike the Sala y Gomez-Nazca ridge system [*Bialas et al.*, 2000] or the Cocos-Carnegie Ridges [*Lonsdale and Klitgord*, 1978], for which enhanced magmatism in the spreading center environment contributed to ridge bathymetric evolution [*Walther*, 2003].

[5] Positive gravimetric anomalies of up to 170 mGal above the magmatic cones of the O'Higgins Group are locally restricted to the volcanic centers. No distinct gravity anomalies indicative of a broader ridge or an existing moat are resolved, however [*Flueh et al.*, 2002]. These results correspond to the inferred absence of a crustal root as indicated by the refraction seismic investigations [*Flueh et al.*, 1998; this study]. The absence of the typical gravimetric pattern as observed along the western extent of the ridge may additionally be masked by the bending and flexure of the Nazca plate as it enters the trench. The "total fusion" age for O'Higgins Guyot is 8.5 ± 0.4 Ma [*von Huene et al.*, 1997]. O'Higgins Seamount was formed at 9 Ma, as inferred from its magnetic signal [*Yáñez et al.*, 2001]. The Miocene magmatic products of the O'Higgins Seamount Group were erupted onto 35.5–36.5 my old oceanic crust [*Yáñez et al.*, 2001]. East of the trench, a prominent magnetic anomaly at 72.6°W/32.7°S indicates the location of the subducted Papudo Seamount. In our study area near the trench, the trend of the Juan Fernández Ridge changes from its nearly W-E orientation (85°) to a more northeasternly direction of 58° (Figure 2). Its eastward projection correlates with a belt of intraslab earthquake hypocenters extending approximately 700 km inland [*Kirby et al.*, 1996]. Reactivation of faults created in an outer-rise setting has been proposed to explain intermediate-depth earthquakes associated with Juan Fernández Ridge subduction [*Kirby et al.*, 1996]. This interpretation is supported by analysis of nodal plane orientations, which correlate to the faulting pattern on the incoming plate (C. Ranero et al., unpublished data, 2003). A reconstruction of the ridge's path into the Chilean Trench documents a change in plate motion at approximately 25 Ma caused by spreading center rotation and plate re-configuration [*Pilger*, 1981, 1983], which triggered a rapid southward migration of the obliquely subducting Juan Fernández Ridge [*Yáñez et al.*, 2001; *Laursen et al.*, 2002]. Recent entrance into the subduction zone occurs near 33°S, roughly parallel to the current direction of plate motion [*Yáñez et al.*, 2001].

3. Data Acquisition and Processing

[6] The easternmost extent of the Juan Fernández Ridge was investigated in detail during the course of the SPOC field campaign using RV SONNE in 2000 [*Reichert et al.*, 2002; *Flueh et al.*, 2002]. To classify the nature of magmatic activity with reference to other marine volcanic chains and aseismic ridges, O'Higgins Guyot and O'Higgins Seamount were mapped with wide-angle seismic, reflection seismic, magnetic, gravimetric, and hydroacoustic measurements. Here, we present the seismic wide-angle data that were collected along two perpendicular lines across the volcanoes supplemented by high-resolution swath bathymetric images of the entire volcanic group and surrounding seafloor (Figure 2). The two seismic lines P03 and P04 (Figure 3) are 210 and 200 km long, respectively. 27 OBS (Ocean Bottom Seismometers) [*Bialas and Flueh*, 1999] and OBH (Ocean Bottom Hydrophones) [*Flueh and Bialas*, 1996] were placed along profile P03 with an instrument spacing of about 4 km (2.2 nm). Coincident multi-channel reflection data were collected along this profile during a previous cruise [*Reichert et al.*, 2002]. Along profile P04, 23 instruments were deployed with an average spacing of 5.2 km (2.8 nm). The seismic signals were generated by a tuned set of 20 air guns with a total volume of 51.2 liters. Shooting was conducted at an interval of 60 s and a speed of 5 kt, resulting in a mean shot point distance of 154 m. Shooting along both profiles was extended into the trench (Figure 3). The data were recorded after low-pass filtering at a sampling rate of 4 ms or 5 ms, depending on the data logger. Employing a processing sequence adapted to the special data characteristics allowed to further improve the quality of the seismic records. We used a time-gated Wiener deconvolution with a gate length of 2 s. On selected stations (e.g., OBH98 in Figure 4) a dip filter in the fk-domain was applied additionally to suppress noise in the far offset domain. Slope filtering further enhanced the resolution in

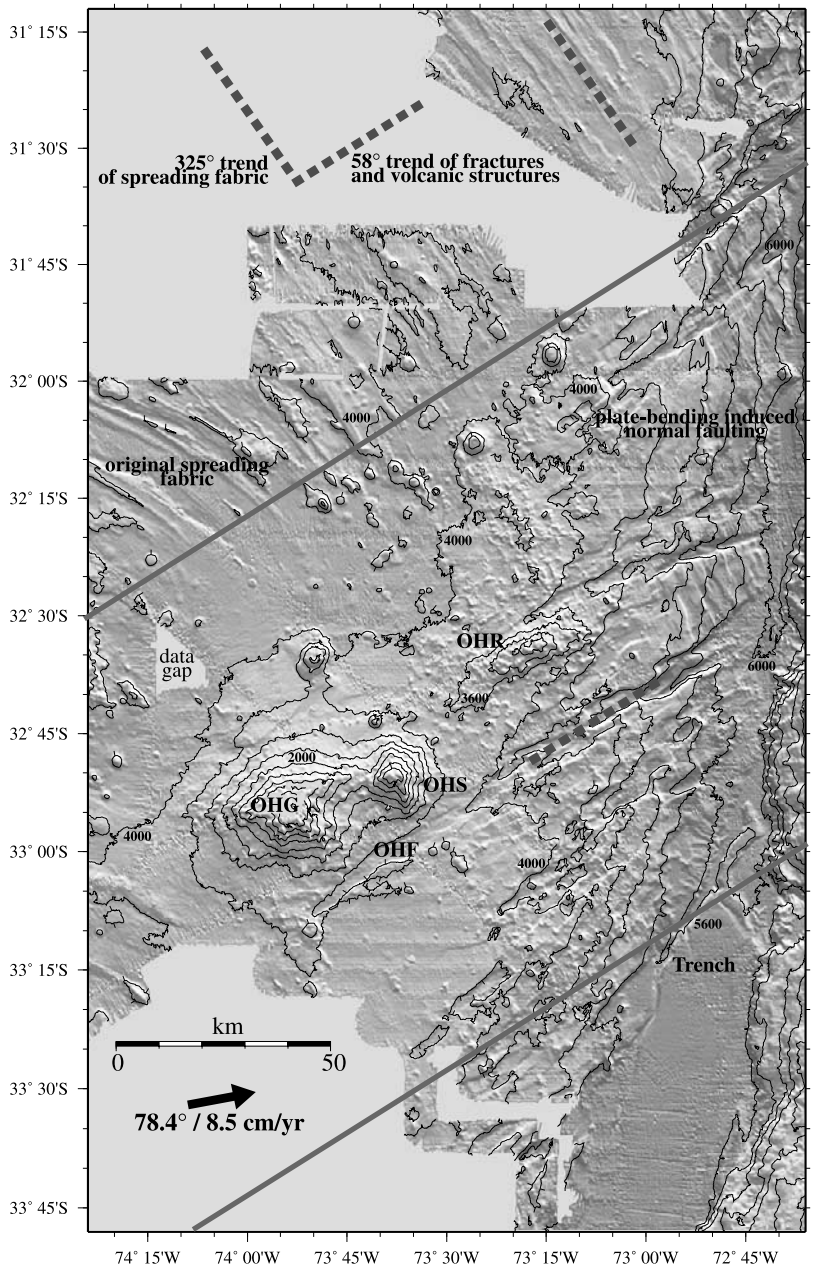

Figure 2. High-resolution bathymetric image of the O'Higgins Seamount Group and Juan Fernández Ridge (JFR). The original spreading fabric is discernible as low-relief ridges terminating north and south of the JFR. The across-width of the JFR (indicated by the thick grey lines) is approximately 140 km. Two sets of fault patterns are recognized: plate-bending induced trench-parallel normal faulting occurs over an area of 30 km across the trench slope. Fracture zones parallel to the trend of the JFR and the volcanic structures affect a broader region of the oceanic crust. The longest fracture zone, the O'Higgins Fracture (OHF) extends ~110 km onto the oceanic plate. Fracture zone trend and spreading fabric trend are extrapolated from the dotted lines. Fractures trend perpendicular to the spreading fabric and represent reactivated inherited structures whose origin is closely linked to the hot spot activity and emplacement of the volcanic structures over the crest of the JFR. The 58° trending fractures are limited to the extent of the JFR. North and south of the ridge crest, fault patterns change direction and are of different origin. See text for further details. OHG: O'Higgins Guyot, OHS: O'Higgins Seamount, OHR: O'Higgins Ridge.

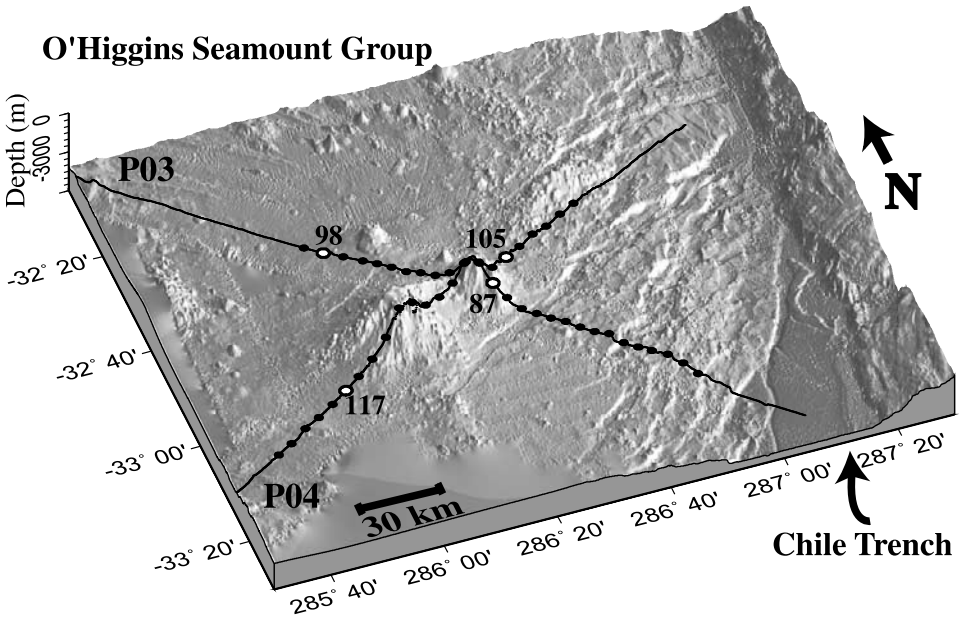

Figure 3. Seismic wide-angle lines P03 and P04 crossing the O'Higgins Seamount Group. Data examples of four stations are shown in Figures 4 and 5 and indicated by their station number and white dots.

the far offset region, helping to identify the crossover of the mantle refraction and lower crustal refraction.

[7] High-resolution hydroacoustic seafloor mapping was conducted continuously (Figure 3) using RV SONNE's onboard SIMRAD EM120 multibeam echo sounder system with a whole angular coverage sector of maximum 150°. Sound velocities were constrained by CTD measurements [*Flueh et al.*, 2002]. The multibeam data collected during cruise SO161 were subsequently merged with existing data collected during previous cruises of RV SONNE (SO103) (Figure 2). Processing of each sweep was carried out using the mbsystem [*Caress and Chayes*, 1996] and Generic Mapping Tools (GMT) [*Wessel and Smith*, 1991] software tools.

4. Morphology of the O'Higgins Seamount Group

[8] O'Higgins Guyot and smaller O'Higgins Seamount are twin volcanoes connected by a low ridge (Figure 2). They are found at approximately 4 km water depth and rise 3.5 km (O'Higgins Guyot) and 2.9 km (O'Higgins Seamount) above the surrounding Eocene seafloor. The conic volumes of the two volcanic edifices best reflect their differences in size: O'Higgins Guyot (~27 km base diameter) has an approximate volume of 668 km^3 ± 10%, whereas O'Higgins Seamount (~15 km base diameter) only has a volume of 177 km^3 ± 10% above average seafloor. Along the trenchward projection of the Juan Fernández Ridge to the northwest, O'Higgins Ridge forms a 9.8 Ma [*Yáñez et al.*, 2001] elongated volcanic structure with a peak elevation of 1 km above the seafloor (Figure 2).

[9] The high-resolution bathymetric data resolves the extent of a network of syngenetic tectonic structures associated with the volcanic centers (Figure 2). The faults run subparallel to the 58° trend of the Juan Fernández Ridge here. The low relief ridge swell near the trench is obscured by the additional elevation of the outer rise. The original spreading fabric, which cannot be identified across the hot spot modified crust around the ridge, best defines its limits (Figure 2), so that the extent of the Juan Fernández Ridge is bordered by the spreading fabric to the north and south. The faults parallel to the hot spot track are restricted to the approximately 140-km-wide ridge swell that has been affected by hot spot magmatic activity. Reactivation of the ridge-related structures occurs between the O'Higgins Group and the trench and reaches offsets that develop more than ~800 m high scarps.

[10] Multiple fault sets have been mapped along the Chilean Trench (C. Ranero et al., unpublished data, 2003). Trench-parallel plate bending-induced normal faulting in the study area covers the lower trench slope but is restricted to the trenchwardmost 30 km, whereas the much better developed ridge-parallel faults extend to a maximum 110 km onto the oceanic crust (e.g., O'Higgins Fracture in Figure 2). A set of non-trench parallel faults occurs north of 29°S, but its origin cannot be linked to hot spot modified lithosphere. We favor a syngenetic origin of the O'Higgins fault pattern associated with the hot spot related emplacement of the eruptive features. Loading-induced plate flexure plays a minor role along this segment of the Juan Fernández Ridge, as discussed below, thus making a solely flexural weakening of the lithosphere unlikely.

[11] The 325° trending seafloor spreading fabric of the oceanic crust documents a spreading direction roughly

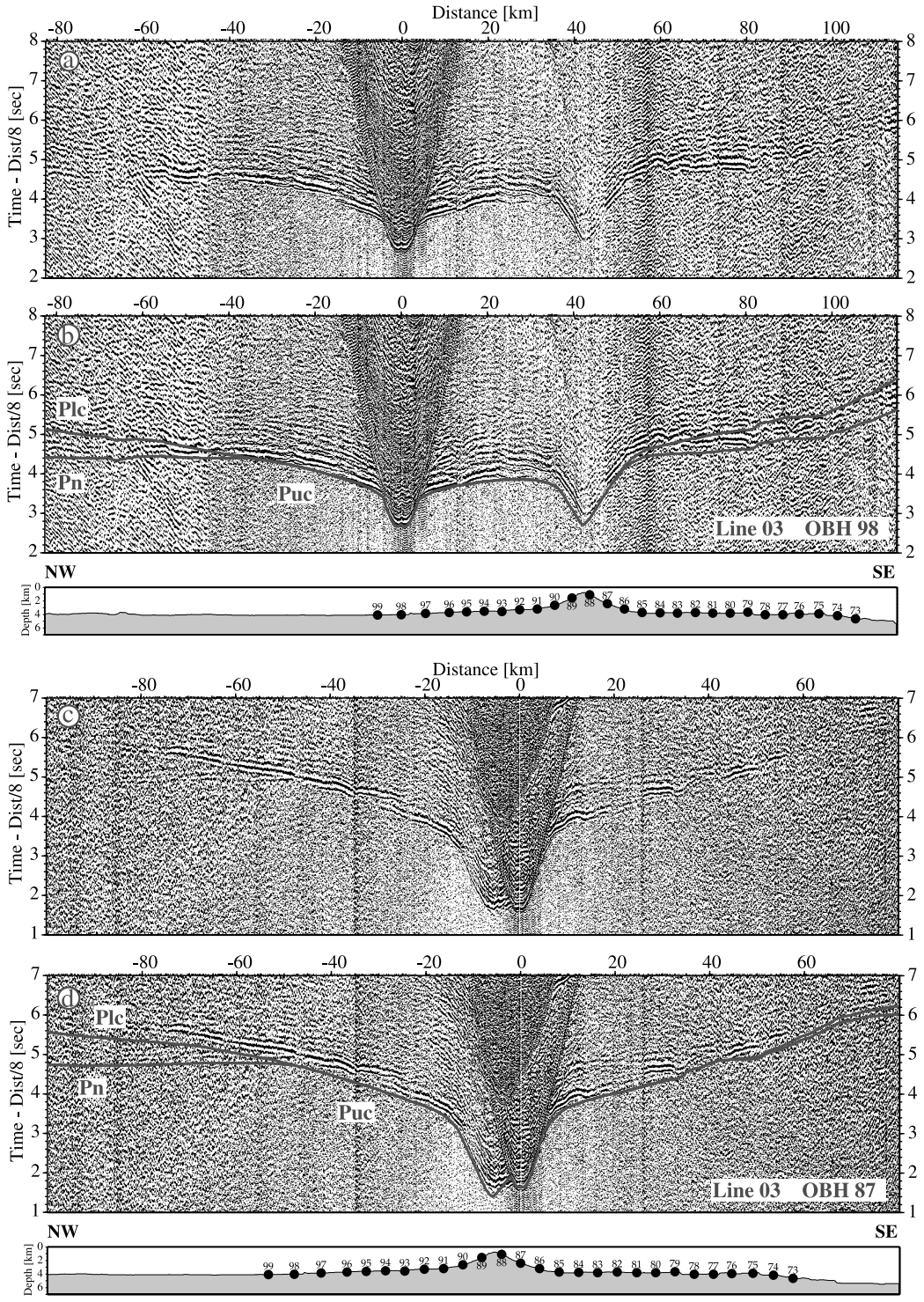

Figure 4. Seismic wide-angle sections for OBH98 (upper images) and OBH87 (bottom images) of line P03, where 27 instruments were deployed. (b) and (d) illustrate the calculated travel times on top of the seismic data shown in (a) and (c), respectively. Travel times are affected by the pronounced morphology of O'Higgins Seamount. The SE segment of the profile is influenced by the deepening seafloor of the trench slope, resulting in slow apparent velocities. Clear phases from the lower crust (Plc) and mantle (Pn) to offsets reaching more than 80 km are observed on the oceanward portion of the profile. The tomographic inversion applied to the data employs primary as well as secondary arrivals to include a maximum of travel time information. Consecutive inversion of different phases using a top-to-bottom approach recovered crustal and mantle velocities successively.

parallel to the fracture zone trend (Figure 2). A tensile stress field perpendicular to the spreading direction has been proposed for the Pacific region [*Winterer and Sandwell*, 1987; *Sandwell et al.*, 1995]. The overall compressive stress regime of an oceanic plate generally inhibits tectonic deficiencies of the lithosphere [*Hieronymus and Bercovici*, 2000]. Local perturbations of the stress field, however, such as a hot spot generated volcanic feature, will lead to a mechanical weakening of the lithosphere [*Hieronymus and Bercovici*, 2000], which will tectonically be expressed as cracks or faults. A focused perturbation of the lithosphere, as observed along the Juan Fernández Ridge, is beneficial to the development of cracks. The focused load of the Juan Fernández Ridge will act as a nucleating flaw and origin for the formation of weak zones propagating in a regional stress field [*Kopp and Phipps Morgan*, 2000]. The pattern of faults around the O'Higgins Group most likely results from inherited defect structures, which develop parallel to the spreading direction in the regional tensile stress field and are reactivated upon the plate's entrance into the trench. Similar fractures have not been reported for larger aseismic ridges currently being subducted, like Cocos Ridge [*Walther*, 2003], or Nazca Ridge [*Hampel et al.*, 2004], due to their non-focused, much broader diffuse distribution of magmatic penetration above these hot spots. The immensely thickened crust of these aseismic ridges (>15 km) will furthermore inhibit a sharp flexural bending into the trench.

5. Tomographic Inversion Scheme

[12] The seismic record sections (examples presented in Figures 4 and 5) show a uniform data quality along the two refraction lines. Clear recordings are present on most station records with offsets exceeding 90 km (e.g., OBH98 and 87 in Figure 4.) Seismic travel times are strongly affected by the morphology of the volcanic edifices, which causes drastic changes in apparent velocities. The plate bending and ridge-and-trough morphology, as well as the adjacent trench, lead to an "asymmetry" in apparent velocities in the record sections with reduced apparent velocities dominating the trenchward portion of the profiles. Along the western parts of the profiles, which extend onto the abyssal seafloor, the upper crustal refraction (*Puc*), lower crustal refraction (*Plc*) and mantle refraction (*Pn*) can be clearly differentiated on almost every station and reveal relatively smooth interval velocity structures. Wide-angle *PmP* Moho reflections are recognized on a number of record sections (e.g., OBH87 in Figure 4).

[13] We employed the FAST tomography code [*Zelt and Barton*, 1998] for our investigations. This method is a first-arrival tomography [e.g., *Nolet*, 1993] utilizing the "regularized inversion" on a uniform velocity grid. The velocity models are gridded to 2 km $\times$ 0.5 km cells in the x and z directions. Using this code for a standard first arrival tomography scheme, however, would only include the *Puc* and *Pn* phases and thus primarily account for the upper crust and mantle, therefore disregarding nearly 1/3 of the travel time information. Because the lower crustal phases (*Plc*) are "covered" as second arrivals behind the first arrival *Pn* and thus would be omitted in a standard first arrival tomography, ray coverage of the lower crust would be meager. As distinct lower crustal phases are present in this specific data set as second arrival refractions between approximately 40 km and 100 km offset (i.e., *Plc*), we chose a hybrid approach to incorporate all crustal and mantle refractions in the final multi-step tomography [*Kopp et al.*, 2003]. For line P03, we were able to use a total of more than 23,500 picks for the inversion. Along P04, more than 12,500 picks were included.

[14] We started by inverting all crustal refractions, disregarding the mantle phases. The rays through the crust include first arrivals up to ~25 km offset (*Puc* in Figures 4 and 5), which merge with gradually increasing velocities into the lower crustal *Plc* refractions. As input model, a minimum-structure velocity model [*Kissling et al.*, 1994] of "normal" oceanic crust with laterally constant v(z) functions was used. The input models for the two profiles account for the known bathymetry of the volcanic domes and include a realistic 2D structure across the O'Higgins volcanoes as displayed in Figure 6. As the mantle phases were omitted in this step, the input models consequently show a crust of infinitive thickness and no sharp velocity step as would be expected across the crust-mantle boundary (Figure 6). The FAST code includes a forward calculation technique that is capable of handling large velocity contrasts [*Hole and Zelt*, 1995], however, a grid-based inversion generally seeks a smooth solution to fit the observed travel times and will fail to resolve sharp velocity contrasts. A "layer stripping" approach, which has been shown to improve the resolution of the computed inversion image [*Kopp et al.*, 2003], did not enhance the crustal inversion quality here. Thus we inverted the oceanic crust by including crustal phases (first and later arrivals) to their maximum offset. The crustal velocities were then held fixed in the next iterations. For the subsequent inversion of mantle velocities, the depth of the Moho was identified using the mantle phases *PmP* and *Pn* in a forward ray tracing approach. This boundary was then held constant during an inversion of the mantle refraction *Pn* to recover upper mantle velocities.

6. Input Model Assessment

[15] To assess the effect of alternative starting models on the stability of the final tomographic output [e.g., *Zelt and Barton*, 1998; *Korenaga et al.*, 2000; *Zelt et al.*, 2003], data inversion was conducted based on different velocity gradients in the subsurface. The aim of the linearization is to detect small-scale velocity perturbations to the input model. Thus the assessment of deviating input models is crucial to the credibility of the final output. Three alternate input models for profile P03 are presented in Figures 6a–6c with variable linear-gradient v(z)-functions in the upper and lower crust (Figure 6d). The final tomographic models derived from using crustal phases only (right panels of Figure 6) show an extremely stable velocity structure in the central parts of the profiles, which are independent of the starting model. The high velocity gradient in input model 1 is justified for the upper crust, as the 6.5 km s^{-1} isoline is kept at a comparable depth

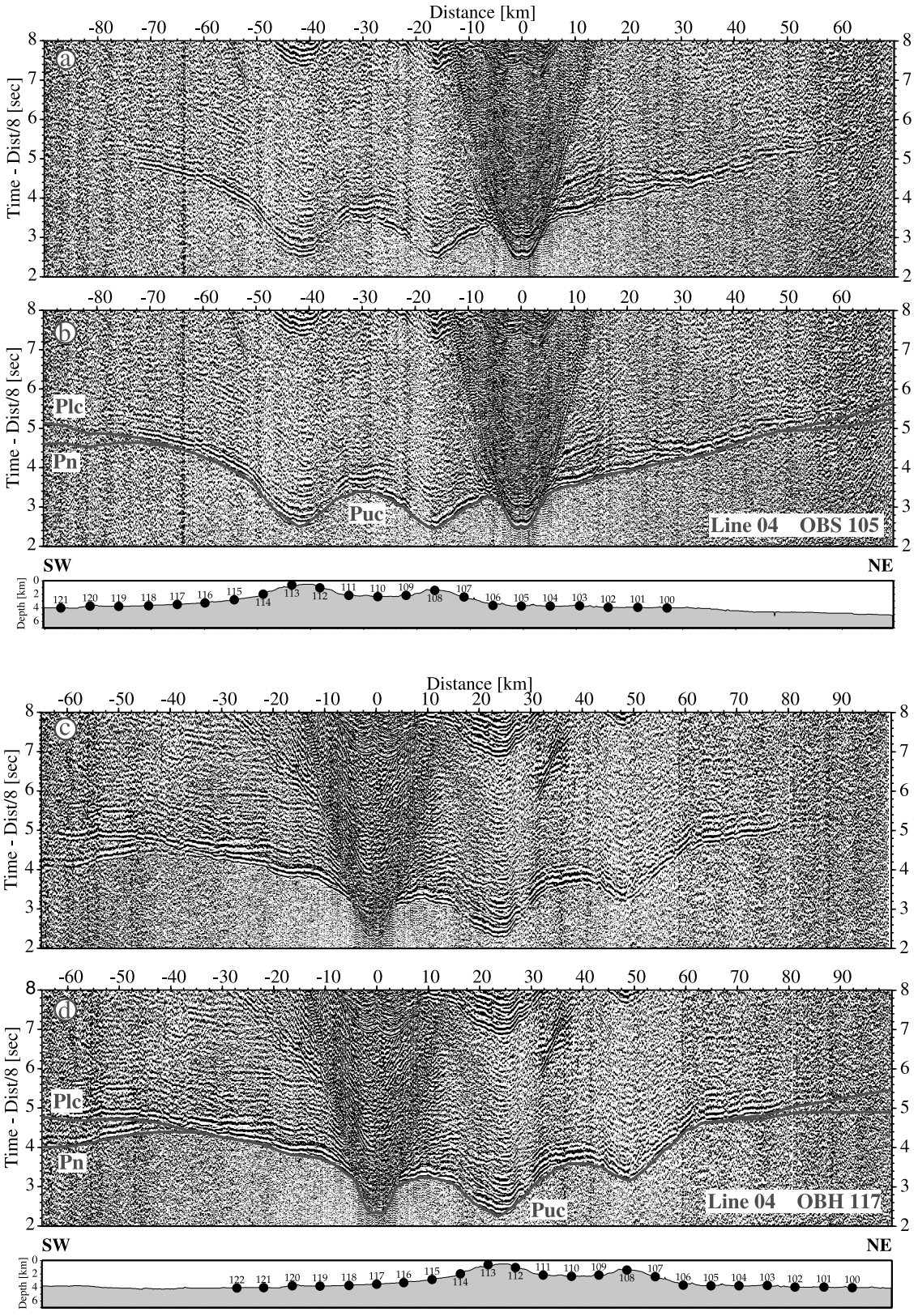

Figure 5. Seismic wide-angle sections for OBS105 and OBH117 of line P04 across O'Higgins Guyot and O'Higgins Seamount. See Figure 4 caption for display information. 23 instruments were deployed along this profile and are indicated with their station number as black dots along the morphology sections. Refer to text for further details.

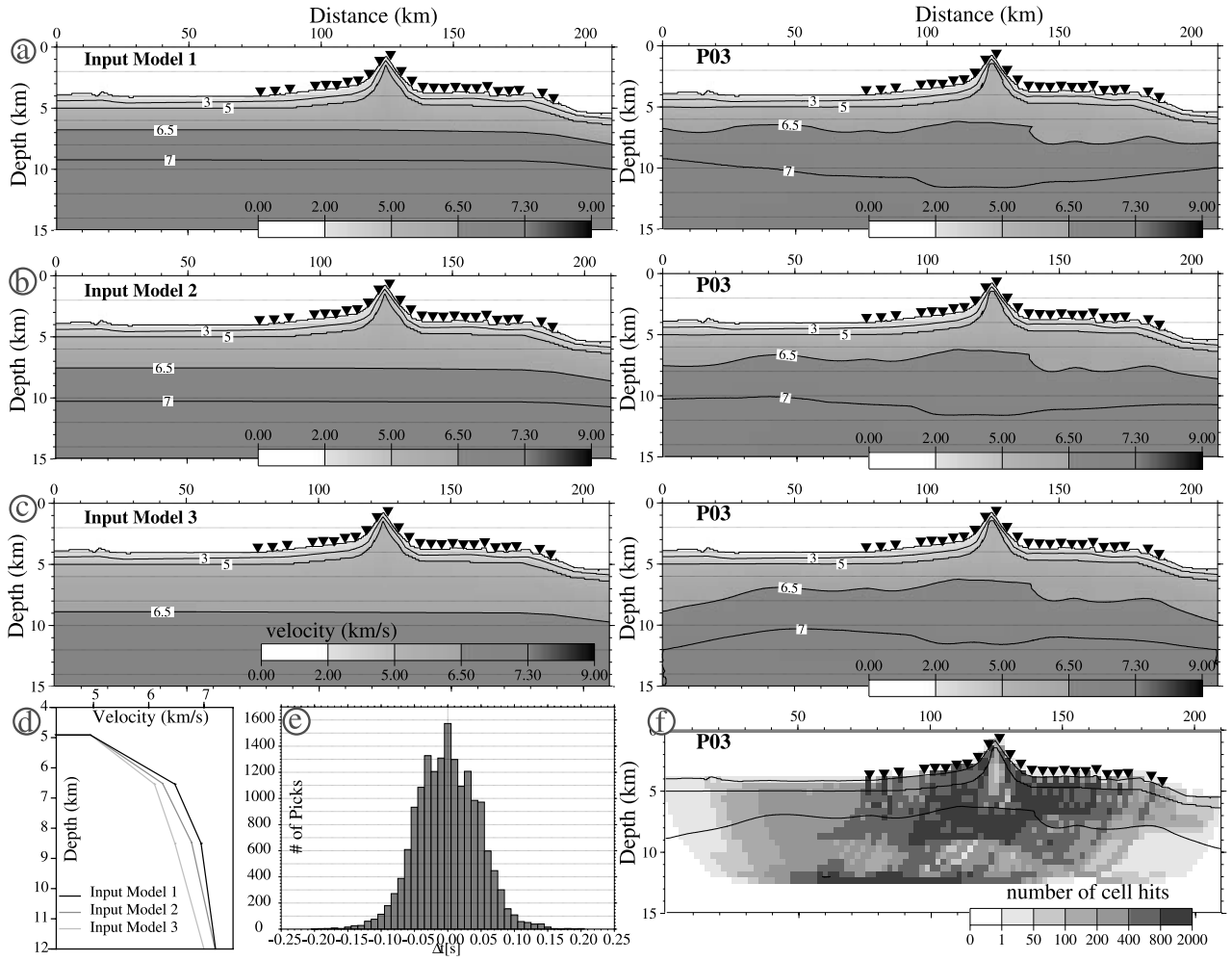

Figure 6. Assessment of different starting models (right panels of (a)–(c)) on the inversion of P03 using crustal arrivals. Tomographic output for the three input models is shown in the left panels of (a)–(c). The input models contain different velocity gradients in the upper and lower crust as displayed in (d). Based on forward modeling, the 3 km/s and 5 km/s isolines are kept identical for all input models. As mantle phases were omitted during this stage of the inversion, the models display a crust of infinite thickness. Topographic information is included in the starting models. The inversion outputs display almost identical results for each input in the central part of the model. The shifting of the velocity isolines is evident at both end segments of P03 as the inversion adjusts the velocity field. The output for input model 2 is least biased to the starting model and is thus chosen as the preferred starting model. Residuals for model 2 are displayed in (e) and are representative for all input models. A nearly homogeneous ray coverage for the inversion cells was achieved underneath the instrument layout with a maximum coverage of up to 2000 hits per cell (Figure 6f). Ray coverage decreases towards the outer limits of the profile. These tests verify that the inversion algorithm is robust and largely independent of the input model for this data set.

(Figure 6a). For the lower crust, however, the velocity gradient was too steep and the 7 km s^{-1} isoline is moved to greater depth in the tomographic output. The same applies to input model 2, however, to a lesser extent, as the output is not significantly biased from the starting model at any depth (Figure 6b). Thus input model 2 is chosen as the preferred starting model. The credibility of the tomographic inversion is best apparent in the result for input model 3, where it is obvious that the velocity gradient in the upper and lower crust was too low. The inversion still yields a robust result for the central part of the profile where ray coverage is sufficient (Figure 6c). This is verified by the shifting of the velocity isolines to shallower depths; data coverage in the line periphery is not

competent to adjust the velocity field. Underneath the instrument layout, however, station density and data quality of the SPOC data set are adequate to yield a stable tomographic inversion.

7. Synthetic Resolution Tests

7.1. "Checkerboard" Test

[16] Prior to calculation of the final refraction tomography, a series of synthetic data tests was performed to assess the lateral model resolution. A ''checkerboard'' test was used as a basis to evaluate the optimal inversion parameters for a reliable resolution of each inversion (Figure 7). An alternating velocity anomaly pattern of positive and negative velocity squares (±5% in the upper 10 km, ±3% below 10 km) is superimposed on the preferred starting model in order to yield a known model with the source-receiver geometry and morphology of the experiment. Synthetic data were calculated from this model, which should recover the anomaly pattern. As this velocity pattern is unrealistic for any natural conditions, the assessment of the retrieved anomaly sequence will solely yield an overview of the data's ability to resolve anomalies of the given size throughout the model dimension [*Zelt and Barton*, 1998]. As is to be expected, the resolution breaks down in the line periphery (Figure 7) where ray coverage is inadequate, while the 20×4 km alternating pattern is resolved in the central portion of the model over the entire depth range.

7.2. Distinct Anomaly Test

[17] A ''checkerboard'' test is an adequate tool to gain a synopsis of the resolution capability for the entire model range, but is insufficient to verify specific isolated anomalies that are expected to be resolved by the tomographic inversion. To evaluate distinct perturbations, we chose a second approach. The target of the tomographic investigations is twofold: (1) to determine the ratio of upper to lower crustal thickness and thus gain insight to possible formation scenarios of the O'Higgins volcanoes and (2) to explore mechanisms associated with or originating from the seamount group's pending entrance into the Chilean Trench. The relation of upper to lower crustal thickness is witness to the magmatic evolution sequence, where extrusives will thicken the upper crust, while plutonic rocks will thicken the lower crust [*Flueh et al.*, 1999]. Possible additional underplating below the seismic Moho will show velocities between typical crustal and mantle values.

[18] A simulation of velocity perturbations in the upper and lower crust was the target of the second synthetic test. We added isolated velocity perturbations on the preferred starting model of line P03 (Figure 7b) and from this calculated synthetic travel times with a source-receiver geometry and coverage of travel time picks corresponding to the SPOC experiment (Figure 8). The anomalies, which were to be retrieved by the inversion, include elevated velocities under the volcanic cone and reduced velocities in the lower portion of the upper crust between the igneous body and the trench in the vicinity of the ridge-and-trough morphology. The preferred input model for P03 (input model 2) was used as a starting model for which the crustal velocities were extrapolated to a depth of 40 km since mantle phases will be disregarded as described earlier. The difference between the model used for synthetic travel time calculation and the preferred starting model for the inversion (as displayed in Figure 6b) is shown in Figure 7b. The isolines displayed in Figure 7 are taken from the final inversion results to indicate the location of the synthetic anomalies with respect to real velocity perturbations gained from the inversion. The difference between the final inversion output gained after six iterations and the preferred starting model is displayed in Figure 7c. The two smaller anomalies are successfully resolved in position and shape. The positive anomaly re-gains more than 90% of the amplitude values, whereas the negative anomaly successfully retrieves 85% of the amplitude values. The ray coverage along profile P03 (Figure 7d) explains why the large anomaly to the northwest is not completely retrieved. Overall, the geometry and instrument spacing of the campaign yields a high resolution of structural anomalies underneath the central part of the profile, and to some extent also in the line periphery. The tomographic inversion scheme used here does not produce artifacts, as is obvious from the synthetic resolution tests. Further testing showed similar stable results, thus we are confident that the inversion scheme applied to this data set will return a reliable output.

8. Seamount Formation and Crustal Flexure

[19] After evaluating the optimal inversion parameters and the preferred input model, the inversion algorithm was applied to the real data. The final tomographic models for P03 and P04 are shown in Figures 9a and 9b, with the calculated travel times obtained from the inversion plotted on the seismic records in the lower panels of Figures 4 and 5. Except for short-wavelength fluctuations an overall satisfying fit could be achieved between the modeled and observed travel times. The tomographic inversion contrivance encompasses a crustal inversion and a complementary subsequent inversion of the upper mantle, which will leave the crustal segment unaltered [*Kopp et al.*, 2003].

[20] In the vicinity of the O'Higgins Seamount Group, the surrounding seafloor is covered by a thin pelagic sediment blanket, as is discernible from the existing reflection seismic data [*Reichert et al.*, 2002] and from the low seismic velocities (<3 km s^{-1}) in the inversion models (Figures 9a and 9b). Both lines show a homogeneous crustal structure with highly elevated velocities characterizing the volcanic centers. The extrusive formation processes that generated the volcanic group are documented by upward deflection of the upper crust velocity isolines (e.g., the 5 km s^{-1} isoline), which almost mimic the morphology of the volcanic cones and the seafloor relief. The tomographic image of P04 shows two distinct igneous bodies comprising O'Higgins Seamount and O'Higgins Guyot. The ridge-like structure connecting the volcanic cones is not of extrusive origin, but is composed of volcanic debris originating from

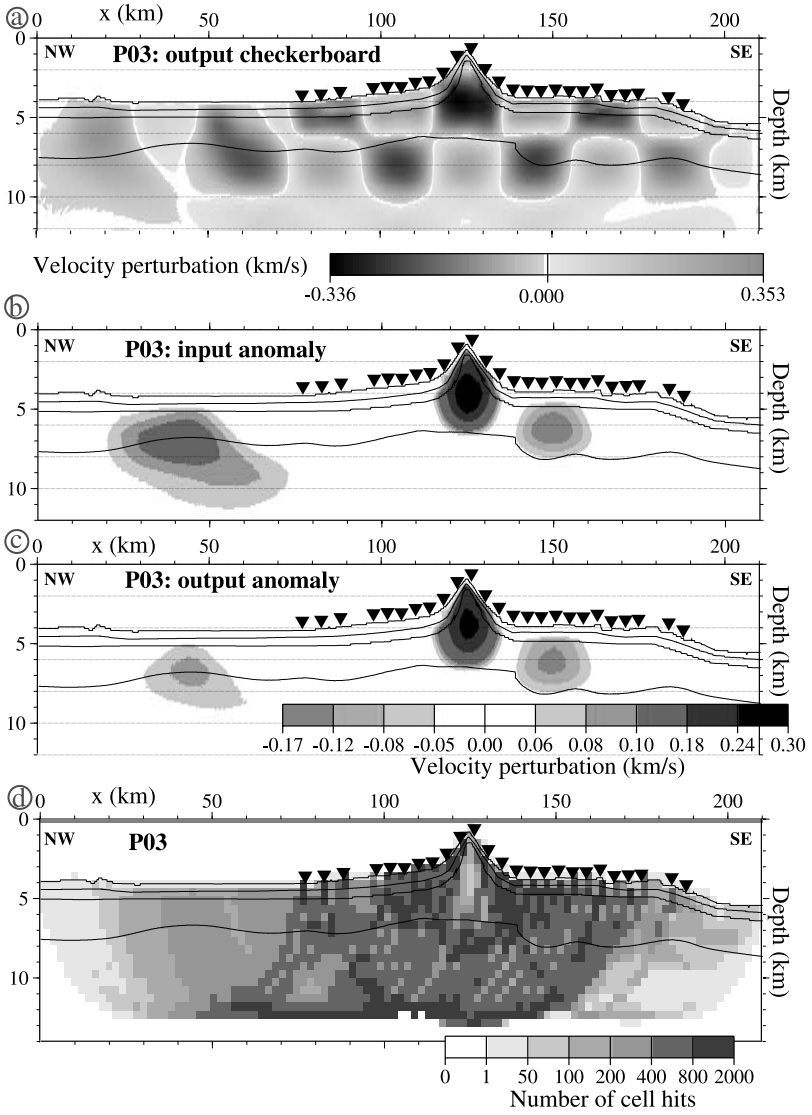

Figure 7. Resolution tests for the tomographic inversion. (a) shows the result of a checkerboard test, i.e., velocity perturbations with respect to starting model. True pattern is ±5% of velocity values contained in the preferred input model in 20 × 4 km squares. Isolines are taken from the final tomography output displayed in Figure 9a. (b) This panel shows the desired inversion velocity update, i.e., difference between the input models for the synthetic travel time calculation and the inversion, respectively. The model difference is characterized by three distinct velocity anomalies, which must be retrieved during the tomography. Extrusive magmatism causes elevated velocities underneath the volcanic edifice with amplitudes of +0.3 km s^{-1}. A lower crustal anomaly of −0.17 km s^{-1} amplitude is located towards the trench, where reduced velocity values are also found in the final inversion output, as indicated by the isoline, which is taken from Figure 9a. A larger third anomaly is located underneath the oceanic basin. (c) displays the difference between the input model and the inversion result. Both anomalies underneath the instrument layout are resolved in position and shape. More than 85% of the amplitude values are retrieved. The third anomaly in the line periphery is not clearly resolved due to lack of ray coverage. (d) shows the number of cell hits achieved during the inversion.

mass wasting processes, as inferred from the low seismic velocities ranging from 3 km s^{-1} to 5 km s^{-1} here.

[21] Along the trenchward southeastern part of line P03, the lower crust is characterized by a raised velocity gradient, where seismic velocities increase to 7.0 km s^{-1}. Along the oceanward segments of the two profiles, a more homogeneous crustal structure of 7 km thickness is resolved with velocities in the lower crust reaching values of 7.1 km s^{-1}.

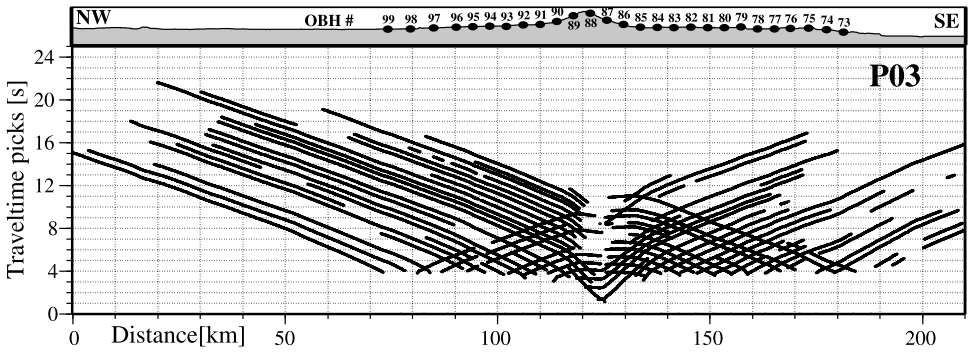

Figure 8. Synthetic travel time picks were generated using the source-receiver geometry and bathymetry of line P03. Coverage of the travel time picks is identical to the real experiment. Random Gaussian noise was added with a standard deviation identical to the estimated pick uncertainties, which are defined individually for every pick (between 0.04 s and 0.12 s; generally increasing with offset). The synthetic data are used for resolution tests (discussed in text) to verify if the crustal velocity anomalies of the test model displayed in Figure 7b may be retrieved with the experiment layout. The smooth input model for the synthetic resolution test is displayed in Figure 6b. Both models are used to image the crust and thus neglect any mantle phases.

[22] The twin volcanoes did not evolve simultaneously, but with a time delay of maximum 0.5 my, as deduced from magnetic modeling [*Yáñez et al.*, 2001]. While the emplacement of the smaller O'Higgins Seamount did not cause a downflexing of the lithosphere, indications for a moat structure and a flexural downbending of the upper crust and lower crust are evident for the larger O'Higgins Guyot on profile P04. Lithospheric flexure has been used in the Pacific region to model elastic thickness and gravity anomalies [*Watts*, 2001]. This is not attempted here, however, due to the strong influence of the neighboring subduction zone and the plate-bending close to the trench. Instead, we compare the O'Higgins situation to existing studies for comparable volcanic settings.

[23] Both volcanoes were emplaced off-axis on approximately 25 Ma lithosphere, for which an elastic thickness T_e = 15 km ± 5 km may be expected [e.g., *Watts et al.*, 1980a; *Bodine et al.*, 1981; *Watts and Ribe*, 1984]. Most previous investigations of lithosphere flexure at seamounts focused on larger loading structures [e.g., *Watts et al.*, 1980b; *Goodwillie and Watts*, 1993]. The O'Higgins Group must be regarded as modest in size compared to other hot spot related volcanic edifices, such as the Great Meteor Seamount, Tenerife, or Hawaii [*Lindwall*, 1988; *Watts et al.*, 1997; *Weigel and Grevemeyer*, 1999]. Seismic investigations of Donizetti Seamount in the Musicians Province north of the Hawaiian chain though indicate a similar moat structure as found underneath O'Higgins Guyot. Donizetti is of comparable dimensions (29 km diameter, 3 km height above surrounding oceanic crust of 7 km thickness) and volume (661 km^3 ± 10%), however was emplaced near a spreading center on young oceanic lithosphere (<5 Ma) [*Kopp et al.*, 2003], for which an elastic thickness of T_e = 5 km was inferred [*Flueh et al.*, 1999]. The flexural bending of the upper crust underneath Donizetti Seamount is also recognized for O'Higgins Guyot and shows similar dimensions. The downflexing of the Moho, however, is much more pronounced for Donizetti than for O'Higgins Guyot. This results from the magmatic emplacement off-axis on the Nazca plate, which leads to a much subdued deflexion because of the higher elastic thickness at time of formation [*Hébert*, 1998].

[24] A similar moat structure as underneath O'Higgins Guyot is not found along profile P03 crossing O'Higgins Seamount. O'Higgins Seamount's lesser volume does not cause a sufficiently large moat structure or downflexing to be resolved. The absence of a moat structure has also been established for a Musicians volcano (HULA Line P03 from *Kopp et al.* [2003]). This volcanic edifice has a slightly larger volume (204 km^3 ± 10%) compared to O'Higgins Seamount and was emplaced on lithosphere for which a much lower elastic thickness may be expected, yet still did not cause resolvable flexural bending of the crust.

9. Upper Mantle Tomography

[25] For the subsequent tomographic inversion of the mantle refraction *Pn*, a "layer-stripping" procedure was chosen, preserving the structural and velocity information above the Moho interface. The bold lines in Figure 9 indicate the depth position of the Moho gained from modeling of *PmP* and *Pn* phases. The lower panel in Figure 9 shows representative ray coverage in the upper mantle, where only shallow penetration is to be expected as the rays travel along the crust-mantle boundary. Testing of various velocity gradients in the upper mantle revealed low values for the gradient here. Inversion resolved areas of highly reduced upper mantle velocities along the two profiles, with values as low as 7.3 km s^{-1}. Tests using varying input velocities yield the same result. Low upper mantle velocities have been found at a number of hot spot related structures, e.g., Hawaii, Gran Canaria, or the Ninetyeast Ridge [*Watts and ten Brink*, 1989; *Ye et al.*, 1999; *Grevemeyer et al.*, 2001]. Magmatic underplating has been inferred to cause these low values,

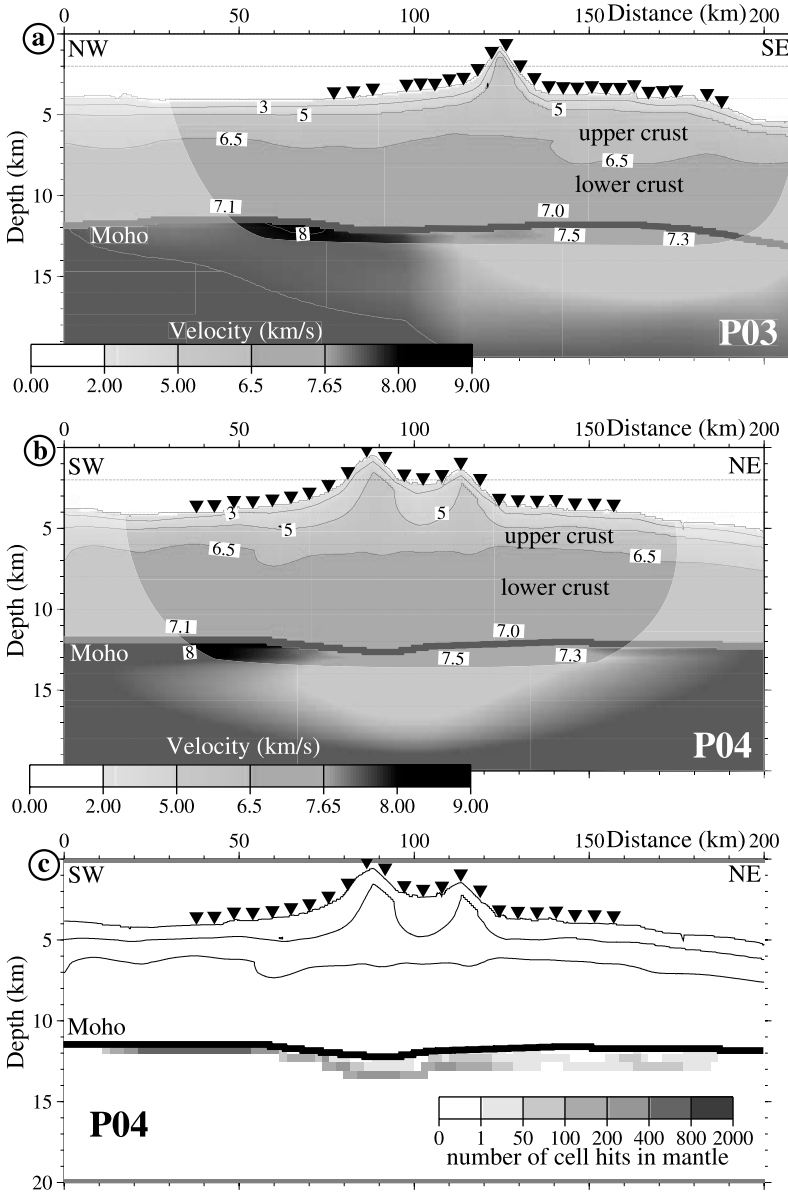

Figure 9. Final inversion models for P03 (a) and P04 (b). The mantle refraction *Pn* was inverted while keeping the crustal segment unaltered. Depth position of Moho is inferred from *PmP* phases. Mantle ray coverage displayed in (c). Regions not sufficiently sampled by ray paths are transparent. Decreased mantle velocities are retrieved along both profiles for the region between the volcanic edifices and the trench, which is characterized by pervasive fracturing (compare Figure 2). Low velocities in this domain are also found in the lower crust along P03 (140–180 km profile distance in (a)). Slight flexural downbending of the upper and lower crust and a corresponding moat structure are caused by the emplacement of O'Higgins Guyot (trend of the 5 km s^{-1} and 6.5 km s^{-1} isolines in (b)). The volume of the smaller O'Higgins Seamount is not sufficient to cause any downflexing.

often supplemented by additional reflections below the Moho reflection [e.g., *Grevemeyer et al.*, 2001], which are not present under the O'Higgins Group.

[26] Some additional constraint on these large-scale upper mantle structures is gained from amplitude evaluations of the *PmP* phases. Here we investigate whether the amplitude variation will invalidate our findings. Amplitudes are very sensitive to small-scale heterogeneities [*Zelt et al.*, 2003], but may be useful in inspecting larger features. Figure 10 shows the record section of OBH 90 on profile P03, which displays a type-example of the onset of the *PmP* phase. The inception of large amplitudes of the *PmP* reflection depends on the velocity contrast across the Moho, the width of the Moho transition zone, and the frequency content of the seismic wave. Increased amplitudes will occur at smaller offsets for a large velocity step. OBH 90

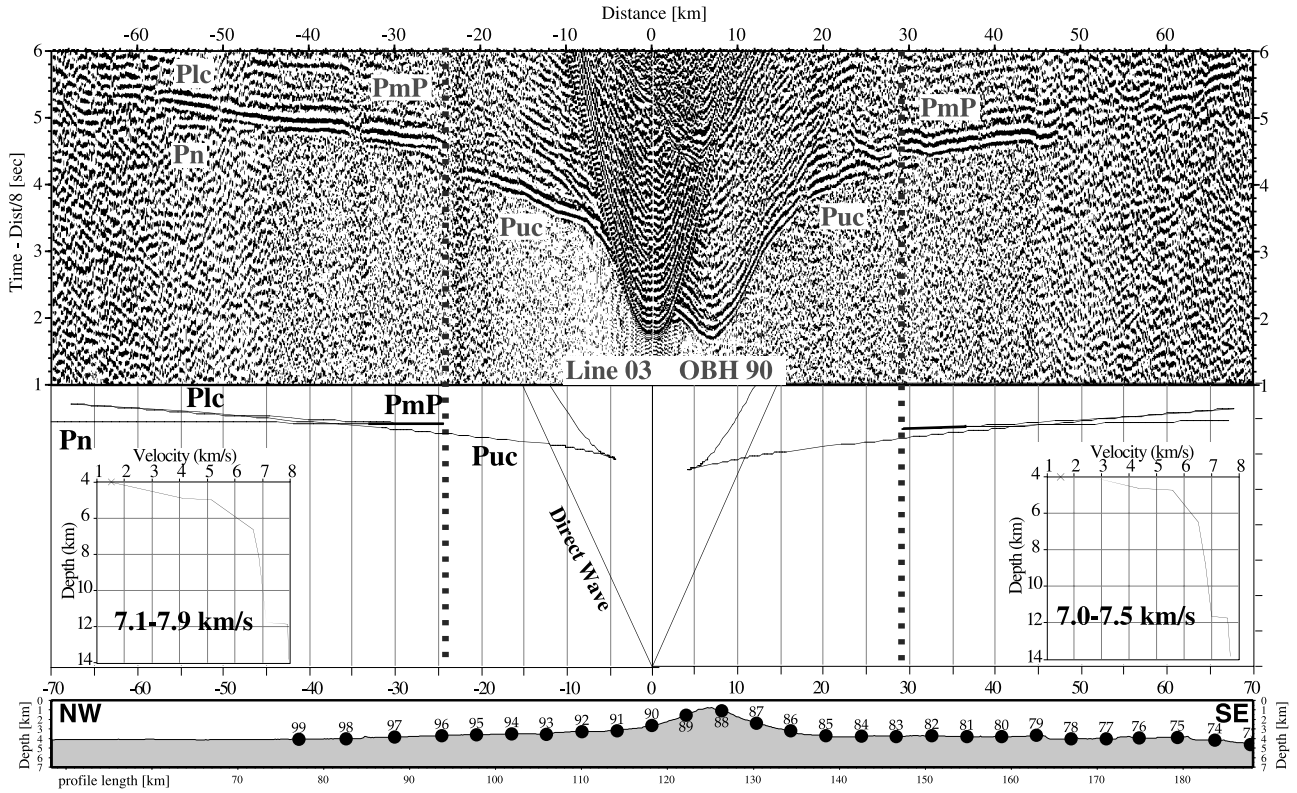

Figure 10. Amplitude evaluations for OBH90. The clear onset of the *PmP* phase occurs at different offsets in the domains of "normal" upper mantle velocities (negative offsets) and decreased upper mantle velocities (positive offsets) as indicated by the stippled black lines. A larger absolute offset of 29 km is expected for a low velocity step across the crust-mantle boundary, whereas 24 km offset are expected for a 0.8 km s^{-1} velocity increase.

is located on the lower northeastern flank of O'Higgins Seamount and thus covers both upper mantle domains. "Normal" velocities are recorded towards the northwestern ocean basin segment, with an increase from 7.1 km s^{-1} above the Moho to 7.9 km s^{-1} below. As shown in the lower panel of Figure 10, the *PmP* is then expected to commence at 24 km offset, which coincides well with the onset seen in the real data (dotted line in Figure 10). The reduced velocities found on the trenchward side (7.0 km s^{-1} to 7.5 km s^{-1}, decreasing to 7.3 km s^{-1} to the southeast) correspond to larger amplitudes at an offset of 29 km.

[27] To lend further credibility to our tomographic results, we conducted independent forward modeling prior to the tomographic inversion in order to seek a minimum-structure model to satisfy the data. Thus model features common to the tomographic and forward-modeling output may be assessed without using subjective a priori information [*Zelt et al.*, 2003]. A comparison of the tomographic inversion and the forward model displays similar structural features (Figure 11). The zone of reduced velocity gradients in the crust along the trenchward part of P03 is also resolved in the forward model, as is the case for the low upper mantle velocities. Along P04, the moat structure southwest of O'Higgins Guyot is resolved by both methods, as are the reduced upper mantle velocities. From forward modeling it is inferred that the minimum depth for the 8 km s^{-1} isoline under the low velocity domain within the upper mantle lies 6 km below the Moho. Even though dissimilarities between the tomographic output models and the result of the forward modeling are recognized, the overall concurrence supports our analysis of the wide-angle data.

10. Provenance of Anomalous Seismic Velocities

[28] Figure 12 shows the velocity-depth distribution underneath the Juan Fernández Ridge. As the tomographic inversion along the two profiles was conducted independently along each line, marginal discrepancies in the velocity fields are observed at the crossing point. Variations due to anisotropy along the two perpendicular striking lines are not observed.

[29] The distribution of the reduced crustal and upper mantle velocities is solely restricted to those areas of the lithosphere that are affected by the pervasive fault pattern subparallel to the ridge (Figure 13). Along profile P04, the transition from the anomalous mantle velocities to common higher values coincides with the termination of the O'Higgins Fracture adjacent to O'Higgins Guyot. The northwestern portion of P03, seaward of the fault pattern extent, does not show anomalous mantle velocity values. This pattern is

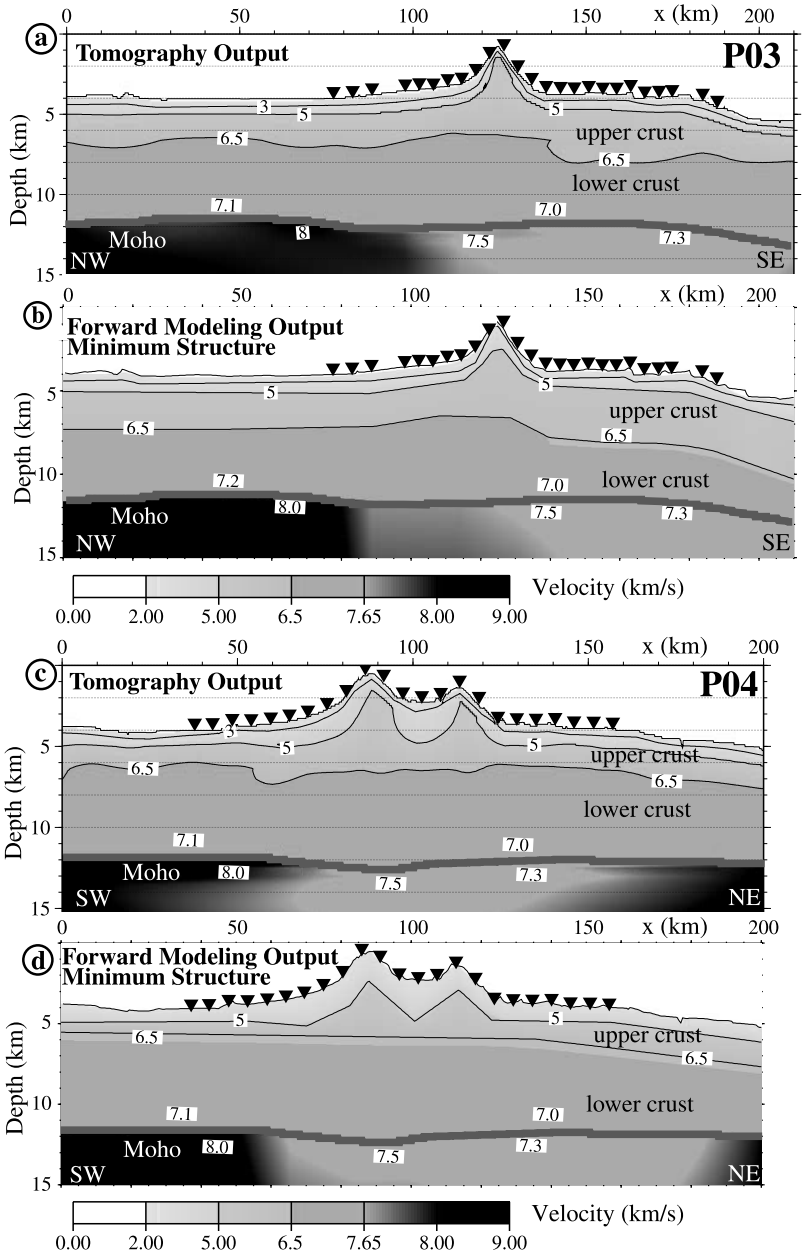

Figure 11. Comparison of tomographic inversion of P03 (a) and P04 (c) to minimum-structure forward models (b) and (d). The main features of the profiles are present in both computations. Position of Moho was held constant during tomography and is thus identical in forward and inversion models. Forward modeling was conducted prior to tomographic inversion without using a priori information other then seafloor bathymetry. Refer to Figure 9 for model areas not sufficiently sampled by paths.

intriguing and suggests a causative relationship between reduced crustal and mantle velocities and the reactivation of inherited structures. The pervasive faulting is imaged in a coincident multi-channel reflection line along P03, however, the downward termination of the faulting is not clear [*Reichert et al.*, 2002; *Flueh et al.*, 2002].

[30] Velocity values intermediate between typical lower crust and mantle velocities (i.e., in the range 7.4–7.8 km s^{-1}) have been mapped for numerous hot spot related volcanic structures (Figure 14) and are commonly attributed to underplating of melt beneath the crust. Underplating generally is focused underneath the volcanic edifice, and an asymmetric distribution is rather uncommon (e.g., Marquesas [*Caress et al.*, 1995]). In the O'Higgins area, reduced velocities are mainly found to the east and south of the dominating volcanoes. A global compilation also reveals that a thickening of the lower crust (oftentimes even expressed as a distinct crustal root, though this is not uniformly developed) generally concurs with underplating, which is not the case for the O'Higgins Group.

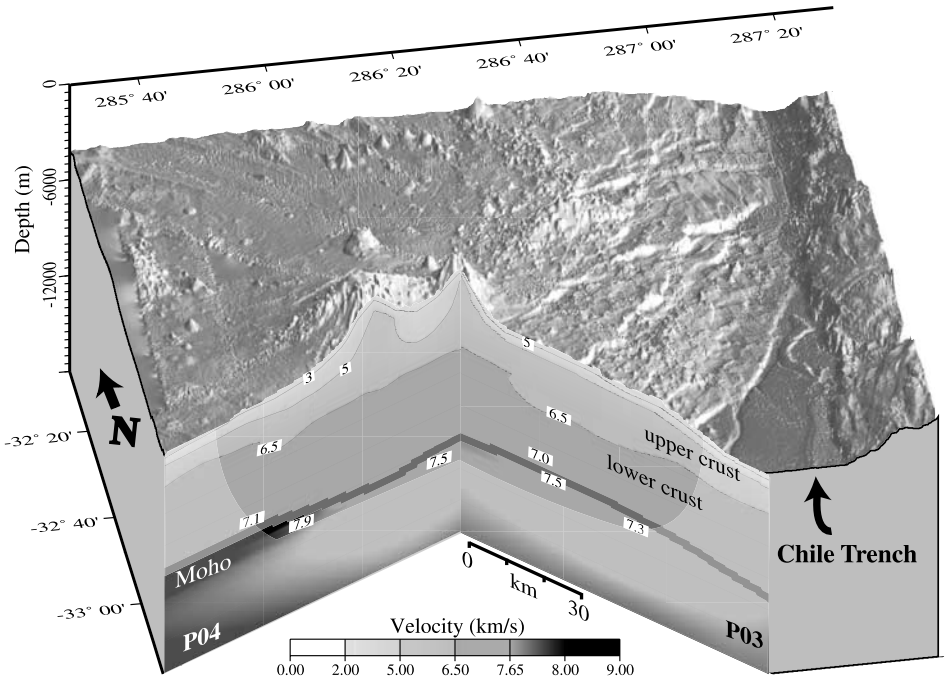

Figure 12. Three-dimensional bathymetric image of the O'Higgins Seamount Group and underlying velocity field. Tomographic inversion of P03 and P04 was conducted independently, resulting in a minor shift of velocity isolines at the profiles' crossing point. Transparent regions are not sampled by ray paths. Decreased upper mantle velocities are only found where seafloor mapping reveals intensive fracturing of the oceanic crust. The fracture pattern is also associated with reduced lower crustal velocities along P03. Low upper mantle velocities cannot be attributed to magmatic underplating, but are most likely caused by hydration of the deformed and faulted oceanic plate.

[31] The modest dimensions of the Juan Fernández Ridge in the study area make underplating for compensation of a flexural load by buoyancy-caused uplift, as suggested by *Watts et al.* [1985] for Hawaii, unlikely. This portion of the Juan Fernández Ridge was generated during a period of subdued magmatic activity, resulting in only isolated volcanic structures along the ridge swell and a ~250 km long gap to the next ridge segment crested with seamounts to the west (Figure 1). This continuous western ridge segment exerts an enhanced load resulting in a pronounced moat [*Sandwell and Smith*, 1997]. It displays an overall different structure than found in the study region resulting from the again intensified magmatic activity.

[32] Reduced mantle velocities may also be associated with magma intrusions at the base of the crust representing magma prevented from penetrating the crust and reaching the seafloor surface during a period of weakened hot spot activity. This pattern would then however be expected across the entire hot spot track and not solely along its trenchward portion, as observed in the study area. Remnants of mafic rocks from an incomplete separation of mafic and ultramafic material have been proposed to be the cause of reduced mantle velocities (>7.6 km s^{-1}) underneath Cocos Ridge [*Walther*, 2003]. Similar differences in composition, however, are inadequate to explain the much lower mantle velocities underneath the Juan Fernández Ridge and would similarly not explain the spatial correlation to the fracture zone pattern.

[33] The low crustal and upper mantle velocities recognized underneath the Juan Fernández Ridge are solely found in connection with the fault zone pattern of inherited defect structures originating from the emplacement of the aseismic ridge and reactivated in the near trench-outer rise setting of the O'Higgins Group. Two additional seismic profiles acquired during the course of the SPOC project north of the O'Higgins Group (SO161-02 and SO161-05) comprise combined on- and offshore refraction data. A east-west trending profile across the entire subduction complex (SO161-02 from *Flueh et al.* [2002]) along latitude 32.08°S (Figure 13) covers oceanic lithosphere still influenced by the pervasive fault pattern and reveals a crustal thickness in excess of 6.8 km. Refraction modeling (H. Kopp et al., manuscript in preparation, 2004) yields reduced velocities in the oceanic crust and upper mantle corresponding to the values presented here. Low P wave velocities again coincide with the inception of reactivated inherited fractures.

[34] Plate-bending induced normal faulting has been documented for numerous outer rise settings in the circum-Pacific [*Masson*, 1991; *Kobayashi et al.*, 1998; *Ranero et al.*, 2003]. Normal faulting is also observed on the Chilean outer rise to the north of the study area (around 31°S [*Reichert et al.*, 2002]), however, is much less devel-

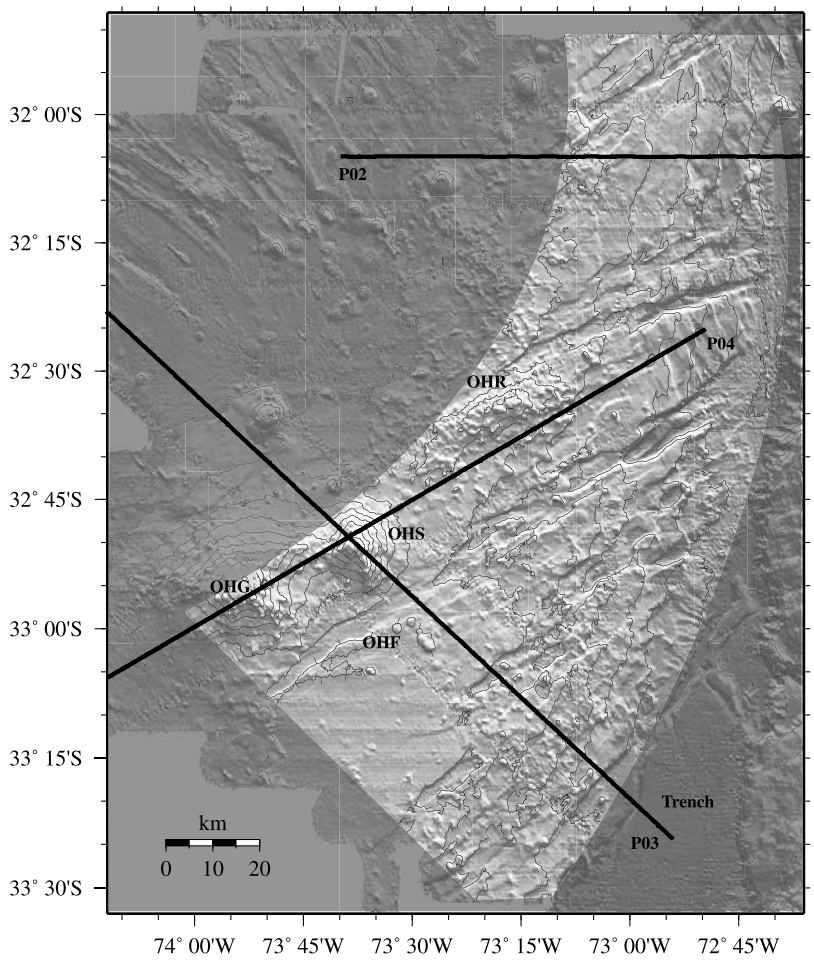

Figure 13. The occurrence of reduced crustal and upper mantle velocities in the study region is indicated by the highlighted area. The velocity distribution is inferred from wide-angle seismic data and is restricted to the hot spot track where the modified lithosphere of the Juan Fernández Ridge shows a pervasive fault pattern (compare Figure 2). As our seismic profiles terminate in the sediment-flooded trench south of the ridge, a continuation of the reduced velocity pattern underneath the trench here remains unclear. Around 32°S, the velocity model is confirmed by data along P02.

oped here as the faulting commences closer to the trench. Reduced uppermost mantle velocities may definitely be precluded for this area, as inferred from the northernmost on-offshore seismic refraction experiment (SO161-05) [*Flueh et al.*, 2002; H. Kopp et al., manuscript in preparation]. The wide-angle data confirm upper mantle velocities in excess of 8.0 km s^{-1} as a lower bound from *Pn* mantle refractions with offsets reaching 150 km. The lithosphere along this transect has been modified to a much lower degree by the reactivation of faults in the outer rise setting than observed across the Juan Fernández Ridge. The crustal thickness of 6.3 km found here may be expected for lithosphere originating at a fast spreading center [*Grevemeyer et al.*, 1999].

11. Hydration of Oceanic Lithosphere

[35] We propose hydration of the oceanic plate as a possible cause for the reduced velocities found underneath the Juan Fernández Ridge. Mineral alteration will modify seismic velocities and lower the density compared to normal lithosphere [*Hess*, 1962]. Hydration has been documented to occur in near-spreading environments [e.g., *Detrick et al.*, 1993; *Canales et al.*, 2000], but is unlikely to appear at the fast-spreading East Pacific Rise, where crustal tectonic processes play a minor role above shallow permanent magma chambers [*Cannat*, 1993]. Near-trench fault-zone hydration of mechanically flawed lithosphere has been suggested by *Kirby et al.* [1996] for the crust and uppermost mantle. The seismic velocities slower than 7.0 km s^{-1} observed in the lower crust of the Juan Fernández Ridge imply the presence of hydrous minerals. A maximum water content of 1.3 wt % H_2O for partially hydrated lower oceanic crust has been calculated by *Hacker et al.* [2003a] based on a global compilation of physical properties of minerals. A linear decrease in seismic upper mantle velocities with the percentage of alteration to serpentine, brucite, and chlorite has been established by *Christensen* [1966]. Applying the

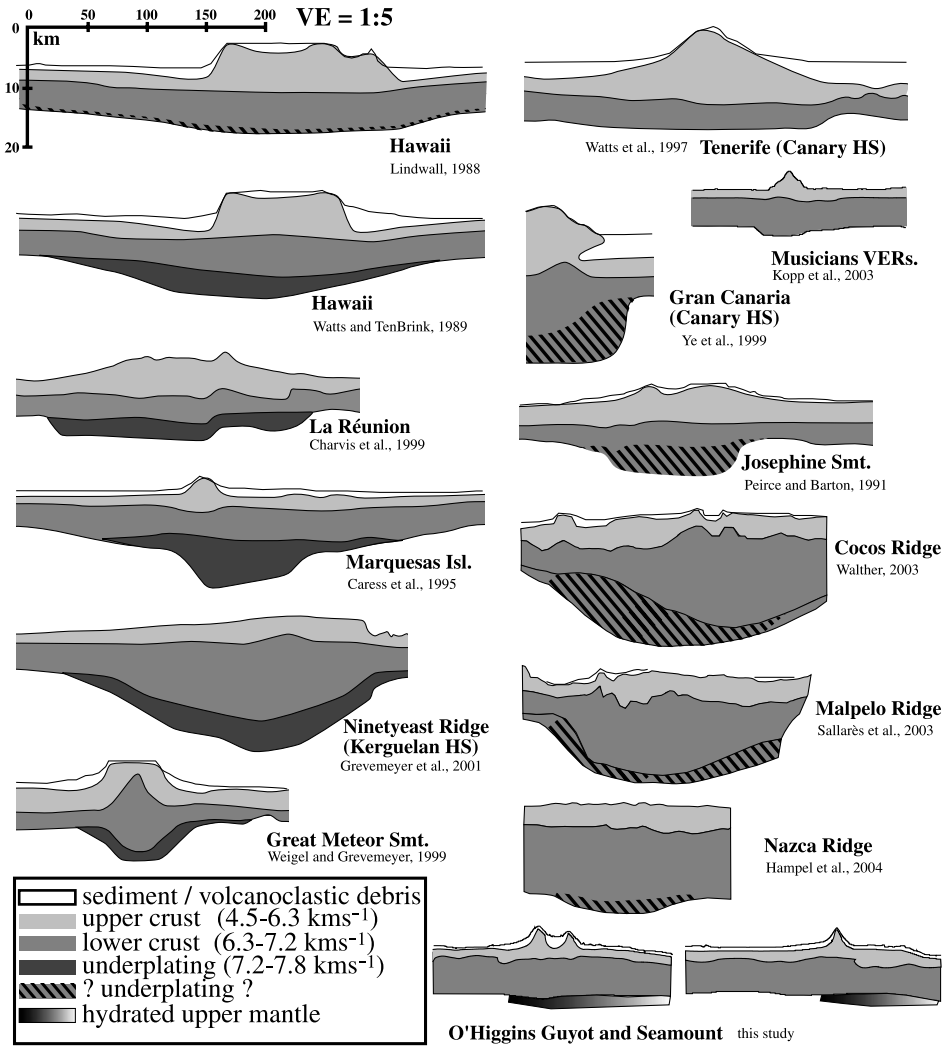

Figure 14. Global compilation of hot spot generated volcanic constructions. Division of upper and lower crust is based on seismic velocities as indicated in the box. Identical scaling applies to all transects. Underplating always coincides with intrusive volcanism and a thickening of the lower crust (La Réunion may be an exception as an enhanced lower crust is not well resolved). Underplating and lower crustal thickening are precluded for Tenerife. Underplating is also unlikely for the Musicians Volcanic Elongated Ridges (VERs), for which a different evolution mechanism away from a hot spot has been proposed. Low upper mantle velocities have also been documented for the Central and South American aseismic ridges, but cannot unequivocally be attributed to underplating. All of these ridges show a well developed crustal root, though, which can be rejected for the Juan Fernández Ridge in the O'Higgins area.

linear regression of *Horen et al.* [1996], a mean P wave velocity of 7.5 km s^{-1} in the uppermost mantle of our study area corresponds to an alteration percentage of ~13% (19% for 7.3 km s^{-1} and 3.75% for 7.8 km s^{-1}). These estimates correspond to results gained from other seismic investigations of a number of subduction zones [*Graeber and Asch*, 1999; *Kamiya and Kobayashi*, 2000; *Zhao et al.*, 2000; *Seno et al.*, 2001; *Carlson and Miller*, 2003]. *Carlson and Miller* [2003] conclude that the mantle is typically about 15% serpentinized in these margins.

[36] In addition to the severe reduction in seismic velocities with the percentage of serpentinization, a linear serpentinization-density relationship has also been observed [*Carlson and Miller*, 2003]. Densities will however be affected to a much lesser degree than seismic velocities. 20% serpentinization (as a crude upper estimate for our study area) will lead to a decrease in bulk density of approximately 0.15 Mgm^{-3}. This modest change may explain why a broad-scale area of reduced densities coherent with the velocity pattern cannot be resolved by the gravity survey conducted during the SPOC cruise [*Flueh et al.*, 2002].

[37] Hydration along inherited tectonic structures of the Juan Fernández Ridge is accompanied by intense seismic

activity. A local marine seismological network installed on the upper plate and in the outer rise region within the scope of the SPOC project [*Flueh et al.*, 2002] yields a preliminary hypocenter distribution on the oceanic plate that roughly aligns with the hot spot track faults [*Thierer et al.*, 2004]. Hypocenter depths lay in the range of 16 km to 23 km below the seafloor, though further analysis will likely refine this range. The Chilean National Earthquake Catalogue also shows a cluster of events in this area, mainly aftershocks of the April 9, 2001 outer rise earthquake. A similar earthquake clustering has been recorded at the entrance point of the Fisher Ridge into the Middle America trench offshore Nicoya Peninsula, Costa Rica [*Newman et al.*, 2002]. Fisher Seamount is of similar modest dimensions as the O'Higgins volcanoes and is emplaced on 6–7 km thick crust, which does not show indications for a crustal root or thickening [*von Huene et al.*, 2000]. The flexural stress caused by the depression of the oceanic crust into the Middle America Trench is accommodated by the reactivation of zones of structural weakness [*Ranero et al.*, 2003]. While faulting is observed in the outer rise setting in this segment (also actively affecting Fisher Seamount), the thick crust of the adjacent Cocos Ridge to the southeast shows little indications for bending-induced faulting [*von Huene et al.*, 2000]. The pervasive outer rise earthquake activity associated with the subduction of the Fisher Ridge and the Juan Fernández Ridge resulting from hydration processes is not recognized for the larger Cocos Ridge offshore Costa Rica [*von Huene et al.*, 2000] or the Nazca Ridge off Peru [*Kirby et al.*, 1996]. A similar fracture pattern as found on the Juan Fernández Ridge is also not observed for these broad aseismic ridges [*von Huene et al.*, 2000; *Walther*, 2003; *Hampel et al.*, 2004], for which a crustal thickness in excess of 15 km has been inferred (Figure 14). This may be related to the broader magmatic penetration by hot spot ridge interaction, as discussed earlier, which may inhibit lithosphere weakening through the generation of crustal flaws necessary for fault reactivation linked to seismogenesis.

[38] *Peacock* [2001] and *Yamasaki and Seno* [2003] discuss hydration/dehydration processes in the deeper mantle in correlation to double seismic zones, which are not observed in central Chile [*Kirby et al.*, 1996]. Deep hydration (several tens of kilometers) of the mantle is unlikely underneath the Juan Fernández Ridge, where the seismicity pattern of the subducting slab correlates spatially to dehydration embrittlement in the crust and uppermost mantle, as inferred from thermal-petrologic models by *Hacker et al.* [2003b]. The wide-angle results of the SPOC study imply a minimum depth of mantle hydration of 6 km below the Moho as a possible uppermost location for the 8 km s^{-1} isoline.

12. Conclusions

[39] Tomographic investigations of the Juan Fernández Ridge reveal a magmatic origin dominated by extrusive processes for the O'Higgins Seamount Group. The ridge segment currently being subducted offshore Valparaiso was likely formed during a period of subdued magmatic activity, resulting in volcanic edifices modest in size. O'Higgins Guyot causes a flexural downbending of the crust and an associated moat structure. The crust-mantle boundary, however, is affected to a lesser extent, due to the limited load of the volcano. This may be a result of a varying elastic thickness in the upper and lower crust, as discussed by *Watts* [2001]. The volume of the smaller O'Higgins Seamount is too low to have caused flexural bending of the 27.5 my old oceanic crust it penetrated.

[40] The off-axis aseismic ridge emplacement caused deficiencies of the lithosphere, leading to faults and zones of weakness. These defect, syngenetic structures are reactivated in the outer rise setting and ridge-parallel fault zones start to develop more than 100 km seaward of the trench. Tomographic inversion of seismic mantle phases reveals reduced uppermost mantle velocities, which correlate to low crustal velocity values and are indicative of mineral alterations in the lithosphere. Uppermost mantle hydration is solely limited to the flexed and faulted lithosphere of the Juan Fernández Ridge and implies a causative relationship with the reactivation of fault zones. Though plate bending induced normal faulting is common along the Chilean outer rise, as revealed by high-resolution bathymetric investigations (C. Ranero et al., unpublished data, 2003), anomalous mantle velocities only occur under the Juan Fernández Ridge and may be precluded for the area north of the ridge. The normal faulting here is not sufficient to cause a deep hydration of the lithosphere. The stronger alteration of the Juan Fernández Ridge crust compared to the segments north and south of the ridge will then solely result from the more intense and pervasive faulting here. While the plate-bending induced trench parallel normal faulting also observed to the north of the ridge extends approximately 30 km onto the outer rise, the deep crustal fault zones characterizing the Juan Fernández Ridge are up to 360% longer and thus affect a much larger area seaward of the trench. Significantly lower mantle velocities could not be resolved in the areas to the north and south where the trench parallel faulting is much less developed and has modified a much smaller area. Hydration processes are not linked to the former hot spot activity or the resulting hot spot modified oceanic crust, but are solely promoted by the pervasive fault pattern found across the Juan Fernández Ridge. The degree and extent of faulting (long faults affecting a larger area of the outer rise across the Juan Fernández Ridge compared to less developed fault zones commencing closer to the trench to the north and south of the ridge) then govern lithosphere hydration.

[41] Hot spot magmatic processes have only moderately added to the crust of the Juan Fernández Ridge, for which a crustal thickening of <1 km is inferred. Normal oceanic crust of 7 km thickness remains buoyant before eclogitization until an age of ~25 my [*van Hunen et al.*, 2002]. Thus only limited increased buoyancy can be expected from crustal thickening of the aseismic ridge, which alone is not sufficient to cause the shallowing of the subduction zone in the flat slab area of Central Chile [*van Hunen et al.*, 2002]. Enhanced buoyancy due to crustal and upper mantle

hydration, however, may represent an important additional mechanism for shallow subduction. The resulting buoyancy effect would be localized along the Juan Fernández Ridge and would not extend into the ridge path's periphery. While the transition from flat to steep subduction is quite abrupt south of the Juan Fernández chain, the shallowing of the Wadati Benioff zone is still recognized for ~550 km to the north [*Cahill and Isacks*, 1992]. A southward migration of the ridge from the northern limit of the flat slab to today's ridge-trench intersection has occurred since 12 Ma [*Yáñez et al.*, 2001]. Recent modeling implies that shallow subduction may be a stable feature even after subduction of a buoyant lithosphere, because the initial shallowing of the slab will inhibit the gabbro-to-eclogite transition, which is essential for the re-steepening of the slab at larger offsets from the trench [*van Hunen*, 2001]. The cooler thermal environment of the shallower portions of the overriding plate, which come into contact with the flat slab, will then defer the gabbro-to-eclogite transition even after passing of the buoyant segment and thus postpone the re-steepening. Though this mechanism may contribute to the Central Chile flat slab, it unlikely is adequate to explain the shallow subduction associated with broader aseismic ridges distributed over wider areas and showing enhanced crustal thickening of Peru or Central America.

[42] **Acknowledgments.** We are grateful to all participants of the SPOC cruise and especially Cpt. Papenhagen and the crew of FS SONNE for the excellent cooperation on board. We would like to thank C. Kopp for discussions on aseismic ridge emplacement and important input. We use the GMT software for many of the figures [*Wessel and Smith*, 1991]. The SPOC project is supported by the German Federal Ministry for Science and Technology (BMBF). Careful reviews by P. Clift and an anonymous reviewer and editorial guidance by O. Oncken are kindly acknowledged.

References

Barazangi, M., and B. L. Isacks (1976), Spatial distribution of earthquakes and subduction of the Nazca plate beneath South America, *Geology*, *4*, 686–692.

Bialas, J., and E. R. Flueh (1999), Ocean bottom seismometers, *Sea Technol*, *40*(4), 41–46.

Bialas, J., N. Kukowski, and Shipboard Science Party (2000), GEOPECO (SONNE Cruise SO-146), Geophysical experiments at the Peruvian continental margin, *Geomar Rep. 96*, Geomar, Kiel, Germany.

Bodine, J. H., M. S. Steckler, and A. B. Watts (1981), Observations of flexure and rheology of the oceanic lithosphere, *J. Geophys. Res.*, *86*, 3695–3707.

Bostock, M. G., R. D. Hyndman, S. Rondenay, and S. M. Peacock (2002), An inverted continental Moho and serpentinization of the forearc mantle, *Nature*, *417*, 536–538.

Cahill, T., and B. L. Isacks (1992), Seismicity and shape of the subducted Nazca plate, *J. Geophys. Res.*, *97*, 17,503–17,529.

Canales, J. P., R. S. Detrick, J. Lin, J. A. Collins, and D. R. Toomey (2000), Crustal and upper mantle seismic structure beneath the rift mountains and across a nontransform offset at the Mid-Atlantic Rdige (35°N), *J. Geophys. Res.*, *105*, 2699–2719.

Cande, S. C., and W. F. Haxby (1991), Eocene propagating rifts in the southwest Pacific and their conjugate features on the Nazca plate, *J. Geophys. Res.*, *96*, 19,609–19,622.

Cannat, M. (1993), Emplacement of mantle rocks in the seafloor at mid-ocean ridges, *J. Geophys. Res.*, *98*, 4163–4172.

Caress, D. W., and D. N. Chayes (1996), Improved processing of Hydrosweep DS multibeam data on the R/V *Maurice Ewing*, *Mar. Geophys. Res.*, *18*, 631–650.

Caress, D. W., M. K. McNutt, R. S. Detrick, and J. C. Mutter (1995), Seismic imaging of hotspot-related crustal underplating beneath the Marquesas Islands, *Nature*, *373*, 600–603.

Carlson, R. L., and D. J. Miller (2003), Mantle wedge water contents estimated from seismic velocities in partially serpentinized peridotites, *Geophys. Res. Lett.*, *30*(5), 1250, doi:10.1029/2002GL016600.

Charvis, P., A. Laesanpura, J. Gallart, A. Hirn, J.-C. Lépine, B. de Voogd, T. A. Minshull, Y. Hello, and B. Pontoise (1999), Spatial distribution of hotspot material added to the lithosphere under La Réunion, from wide-angle seismic data, *J. Geophys. Res.*, *104*, 2875–2893.

Christensen, N. I. (1966), Elasticity of ultrabasic rocks, *J. Geophys. Res.*, *71*, 5921–5931.

DeMets, C., R. G. Gordon, D. F. Argus, and S. Stein (1990), Current plate motions, *Geophys. J. Int.*, *101*, 425–478.

DeMets, C., R. G. Gordon, D. F. Argus, and S. Stein (1994), Effect of recent revisions to the geomagnetic reversal timescale on estimates of current plate motions, *Geophys. Res. Lett.*, *21*, 2191–2194.

Detrick, R. S., R. S. White, and G. M. Purdy (1993), Crustal structure of North Atlantic fracture zones, *Rev. Geophys.*, *31*, 439–458.

Flueh, E. R., and J. Bialas (1996), A digital, high data capacity ocean bottom recorder for seismic investigations, *Int. Underwater Syst. Design*, *18*(3), 18–20.

Flueh, E. R., N. Vidal, C. R. Ranero, A. Hojka, R. von Huene, J. Bialas, K. Hinz, D. Cordoba, J. J. Dañobeitia, and C. Zelt (1998), Seismic investigations of the continental margin off- and onshore Valparaiso, Chile, *Tectonophysics*, *288*, 251–263.

Flueh, E. R., J. O'Connor, J. Phipps Morgan, J. Wagner, and Shipboard Science Party (1999), HULA (SONNE Cruise SO-142): Interdisciplinary investigations on the timing of the Hawaii-Emperor Bend and the origin of lithospheric anomalies along the Musician seamount chain, *Geomar Rep. 90*, Geomar, Kiel, Germany.

Flueh, E. R., H. Kopp, B. Schreckenberger, and Shipboard Science Party (2002), SPOC (SONNE Cruise SO-161 Leg 1 and 4), Subduction Processes off Chile, *Geomar Rep. 102*, Geomar, Kiel, Germany.

Goodwillie, A. M., and A. B. Watts (1993), An altimetric and bathymetric study of elastic thickness in the central Pacific Ocean, *Earth Planet. Sci. Lett.*, *118*, 311–326.

Graeber, F. M., and G. Asch (1999), Three-dimensional models of *P* wave velocity and *P*-to-*S* ratio in the southern central Andes by simultaneous inversion of local earthquake data, *J. Geophys. Res.*, *104*, 20,237–20,256.

Grevemeyer, I., N. Kaul, and H. Villinger (1999), Hydrothermal activity and the evolution of the seismic properties of upper oceanic crust, *J. Geophys. Res.*, *104*, 5069–5079.

Grevemeyer, I., E. R. Flueh, C. Reichert, J. Bialas, D. Klaeschen, and C. Kopp (2001), Crustal architecture and deep structure of the Ninetyeast Ridge hotspot trail from active-source ocean bottom seismology, *Geophys. J. Int.*, *144*, 1–22.

Gudmundsson, O., and M. Sambridge (1998), A regionalized upper mantle (RUM) seismic model, *J. Geophys. Res.*, *103*, 7121–7136.

Hacker, B. R., G. A. Abers, and S. M. Peacock (2003a), Subduction factory: 1. Theoretical mineralogy, densities, seismic wave speeds, and H_2O contents, *J. Geophys. Res.*, *108*(B1), 2029, doi:10.1029/2001JB001127.

Hacker, B. R., S. M. Peacock, G. A. Abers, and S. D. Holloway (2003b), Subduction factory: 2. Are intermediate-depth earthquakes in subducting slabs linked to metamorphic dehydration reactions?, *J. Geophys. Res.*, *108*(B1), 2030, doi:10.1029/2001JB001129.

Hampel, A., N. Kukowski, J. Bialas, C. Huebscher, and R. Heinbockel (2004), Ridge subduction at an erosive margin: The collision zone of the Nazca Ridge in southern Peru, *J. Geophys. Res.*, *109*, B02101, doi:10.1029/2003JB002593.

Hébert, H. (1998), Etudes géophysiques d'une dorsale naissante (dorsale d'Aden à l'Ouest de 46°E) et d'une dorsale fossile (dorsale de Wharton): Implications sur les processus de l'accrétion océanique, et la déformation intraplaque dans l'Océan Indien, Thèse de Doctorat, 372 pp., Univ. Paris 7.

Hess, H. H. (1962), History of ocean basins, in *Petrological Studies: A Volume in Honor of A. F. Buddington*, edited by A. E. Engel, H. L. James, and B. F. Leonard, pp. 599–620, Geol. Soc. of Am., Boulder, Colo.

Hieronymus, C. F., and D. Bercovici (2000), Non-hotspot formation of volcanic chains: Control of tectonic and flexural stresses on magma transport, *Earth Planet. Sci. Lett.*, *181*, 539–554.

Hole, J. A., and B. C. Zelt (1995), 3-D finite-difference reflection travel times, *Geophys. J. Int.*, *121*, 427–434.

Horen, H., M. Zamora, and G. Dubuisson (1996), Seismic waves velocities and anisotropy in serpentinized peridotites from Xigaze ophiolite: Abundance of serpentine in slow spreading ridge, *Geophys. Res. Lett.*, *23*, 9–12.

Jiao, W., P. G. Silver, Y. Fei, and C. T. Prewitt (2000), Do intermediate- and deep-focus earthquakes occur on preexisting weak zones? An examination of the Tonga subduction zone, *J. Geophys. Res.*, *105*, 28,125–28,138.

Kamiya, S., and Y. Kobayashi (2000), Seismological evidence for the existence of serpentinized wedge mantle, *Geophys. Res. Lett.*, *27*, 819–822.

Kirby, S., E. R. Engdahl, and R. Denlinger (1996), Intermediate-depth intraslab earthquakes and arc volcanism as physical expressions of crustal and uppermost mantle metamorphism in subducted slabs, in *Subduction: Top to Bottom*, *Geophys. Monogr. Ser.*, vol. 96, edited by G. Bebout et al., pp. 195–214, AGU, Washington, D. C.

Kissling, E., W. L. Ellsworth, D. Eberhart-Phillips, and U. Kradolfer (1994), Initial reference models in local earthquake tomography, *J. Geophys. Res.*, *99*, 19,635–19,646.

Kobayashi, K., M. Nakanishi, K. Tamaki, and Y. Ogawa (1998), Outer slope faulting associated with the western Kuril and Japan trenches, *Geophys. J. Int.*, *134*, 356–372.

Kopp, C., and J. Phipps Morgan (2000), Is the en-echelon formation of volcanic elongated ridges due to interacting 'dike-like' magma propagation away from discrete volcanic centers?, *Eos Trans. AGU*, *81*(48), Fall Meet. Suppl., Abstract V21F-11.

Kopp, H., C. Kopp, J. Phipps Morgan, E. R. Flueh, W. Weinrebe, and W. J. Morgan (2003), Fossil hot spot-ridge interaction in the Musicians Seamount Province: Geophysical investigations of hot spot volcanism at volcanic elongated ridges, *J. Geophys. Res.*, *108*(B3), 2160, doi:10.1029/2002JB002015.

Korenaga, J., W. S. Holbrook, G. M. Kent, P. B. Kelemen, R. S. Detrick, H.-C. Larsen, J. R. Hopper, and T. Dahl-Jensen (2000), Crustal structure of the southeast Greenland margin from joint refraction and reflection seismic tomography, *J. Geophys. Res.*, *105*(B9), 21,591–21,614.

Laursen, J., D. W. Scholl, and R. von Huene (2002), Neotectonic deformation of the central Chile margin: Deepwater forearc basin formation in response to hot spot ridge and seamount subduction, *Tectonics*, *21*(5), 1038, doi:10.1029/2001TC901023.

Lindwall, D. A. (1988), A two-dimensional seismic investigation of crustal structure under the Hawaiian islands near Oahu and Kauai, *J. Geophys. Res.*, *93*, 12,107–12,122.

Lonsdale, P., and K. D. Klitgord (1978), Structure and tectonic history of the eastern Panama Basin, *Geol. Soc. Am. Bull.*, *89*, 981–999.

Masson, D. G. (1991), Fault patterns at outer trench walls, *Mar. Geophys. Res.*, *13*, 209–225.

Newman, A. V., S. Y. Schwartz, V. Gonzalez, H. R. DeShon, J. M. Protti, and L. M. Dorman (2002), Along-strike variability in the seismogenic zone below Nicoya Peninsula, Costa Rica, *Geophys. Res. Lett.*, *29*(20), 1977, doi:10.1029/2002GL015409.

Nolet, G. (1993), Solving large linearized tomographic problems, in *Seismic Tomography: Theory and Practice*, edited by H. M. Iyer and K. Hirahara, pp. 227–247, Chapman and Hall, New York.

Nur, A., and Z. Ben-Avraham (1981), Volcanic gaps and the consumption of aseismic ridges in South America, *Mem. Geol. Soc. Am.*, *154*, 729–740.

Peacock, S. (1990), Fluid processes in subduction zones, *Science*, *248*, 329–337.

Peacock, S. (1993), Large-scale hydration of the lithosphere above subducting slabs, *Chem. Geol.*, *108*, 49–59.

Peacock, S. (2001), Are the lower planes of double seismic zones caused by serpentine dehydration in the subducting oceanic mantle?, *Geology*, *29*, 299–302.

Peirce, C., and P. J. Barton (1991), Crustal structure of the Madeira-Tore Rise, eastern North Atlantic - results of a DOBS wide-angle and normal incidence seismic experiment in the Josephine Seamount region, *Geophys. J. Int.*, *106*, 357–378.

Pilger, R. H., Jr. (1981), Plate reconstructions, aseismic ridges, and low-angle subduction beneath the Andes, *Geol. Soc. Am. Bull.*, *92*, 448–456.

Pilger, R. H., Jr. (1983), Kinematics of the South American subduction zone from global plate reconstructions, in *Geodynamics of the Eastern Pacific Region, Caribbean and Scotia Arcs*, *Geodyn. Ser.*, vol. 9, edited by R. Cabré, pp. 113–125, AGU, Washington, D. C.

Ranero, C. R., J. Phipps Morgan, K. McIntosh, and C. Reichert (2003), Bending-related faulting and mantle serpentinization at the Middle America trench, *Nature*, *425*, 367–373.

Reichert, C., B. Schreckenberger, and Shipboard Science Party (2002), SPOC (SONNE Cruise SO-161 Leg 2 and 3), Subduction Processes off Chile, BGR report, Bundesanst. fuer Geowiss. und Rohstoffe (BGR), Hannover, Germany.

Sallarès, V., P. Charvis, E. R. Flueh, and J. Bialas (2003), Seismic structure of Cocos and Malpelo volcanic ridges and implications for hot spot-ridge interaction, *J. Geophys. Res*, (B12), 2564, doi:10.1029/2003JB002431.

Sandwell, D., and W. H. F. Smith (1997), Global marine gravity from Geosat and ERS-1 Satellite Altimetry, *J. Geophys. Res.*, *102*, 10,039–10,054.

Sandwell, D. T., E. L. Winterer, J. Mammerickx, R. A. Duncan, M. A. Lynch, D. A. Levitt, and C. A. Johnson (1995), Evidence for diffuse extension of the Pacific plate from Puka-puka ridges and cross-grain gravity lineations, *J. Geophys. Res.*, *100*, 15,087–15,099.

Seno, T., and Y. Yamanaka (1996), Double seismic zones, compressional deep trench-outer rise events, and superplumes, in *Subduction: Top to Bottom*, *Geophys. Monogr. Ser.*, vol. 96, edited by G. Bebout et al., pp. 347–355, AGU, Washington, D. C.

Seno, T., D. Zhao, Y. Kobayashi, and M. Nakamura (2001), Dehydration of serpentinized mantle: Seismic evidence from southwest Japan, *Earth Planets Space*, *53*, 861–871.

Thierer, P., E. R. Flueh, H. Kopp, F. Tilmann, D. Comte, and S. Contreras (2004), Local earthquake monitoring offshore Valparaiso, Chile, *Nueus. Jahrb. Geol. Palaeontol. Abh.*, in press.

Tibi, R., G. Bock, and C. H. Estabrook (2002), Seismic body wave constraint on mechanisms of intermediate-depth earthquakes, *J. Geophys. Res.*, *107*(B3), 2160, doi:10.1029/2001JB000361.

von Huene, R., J. Corvalán, E. R. Flueh, K. Hinz, J. Korstgard, C. R. Ranero, W. Weinrebe, and the CONDOR Scientists (1997), Tectonic control of the subducting Juan Fernández Ridge on the Andean margin near Valparaiso, Chile, *Tectonics*, *16*, 474–488.

von Huene, R., C. R. Ranero, W. Weinrebe, and K. Hinz (2000), Quaternary convergent margin tectonics of Costa Rica, segmentation of the Cocos Plate, and Central American volcanism, *Tectonics*, *19*, 314–334.

van Hunen, J. (2001), Shallow and buoyant lithospheric subduction: Causes and implications from thermo-chemical numerical modeling, Ph.D. thesis, 128 pp., Utrecht Univ., Utrecht, Netherlands.

van Hunen, J., A. P. van den Berg, and N. J. Vlaar (2002), On the role of subducting oceanic plateaus in the development of shallow flat subduction, *Tectonophysics*, *352*, 317–333.

Walther, C. H. E. (2003), The crustal structure of the Cocos ridge off Costa Rica, *J. Geophys. Res.*, *108*(B3), 2136, doi:10.1029/2001JB000888.

Watts, A. B. (2001), *Isostasy and Flexure of the Lithosphere*, 458 pp., Cambridge Univ. Press, New York.

Watts, A. B., and N. M. Ribe (1984), On geoid heights and flexure of the lithosphere at seamounts, *J. Geophys. Res.*, *89*, 11,152–11,170.

Watts, A. B., and U. S. ten Brink (1989), Crustal structure, flexure, and subsidence history of the Hawaiian Islands, *J. Geophys. Res.*, *94*, 10,473–10,500.

Watts, A. B., J. H. Bodine, and N. M. Ribe (1980a), Observations of flexure and the geological evolution of the Pacific ocean basin, *Nature*, *283*, 532–537.

Watts, A. B., J. H. Bodine, and M. S. Steckler (1980b), Observations of flexure and the state of stress in the oceanic lithosphere, *J. Geophys. Res.*, *85*, 6369–6376.

Watts, A. B., U. S. ten Brink, P. Buhl, and T. Brocher (1985), A multichannel seismic study of the lithospheric flexure across the Hawaiian-Emperor seamount chain, *Nature*, *315*, 105–111.

Watts, A. B., C. Peirce, J. Collier, R. Dalwood, J. P. Canales, and T. J. Henstock (1997), A seismic study of lithospheric flexure in the vicinity of Tenerife, Canary Islands, *Earth Planet. Sci. Lett.*, *146*, 431–447.

Weigel, W., and I. Grevemeyer (1999), The Great Meteor seamount: Seismic structure of a submerged intraplate volcano, *J. Geodyn.*, *28*, 27–40.

Wessel, P., and W. H. F. Smith (1991), Free software helps map and display data, *Eos Trans. AGU*, *72*, 441, 445–446.

Winterer, E. L., and D. T. Sandwell (1987), Evidence from en-echelon cross-grain ridges for tensional cracks in the Pacific plate, *Nature*, *329*, 534–535.

Yamasaki, T., and T. Seno (2003), Double seismic zones and dehydration imbrittlement of the subducting slab, *J. Geophys. Res.*, *108*(B4), 2212, doi:10.1029/2002JB001918.

Yáñez, G. A., C. R. Ranero, R. von Huene, and J. Diaz (2001), Magnetic anomaly interpretation across the southern central Andes (32°S–34°S): The role of the Juan Fernández Ridge in the late Tertiary evolution of the margin, *J. Geophys. Res.*, *106*, 6325–6345.

Ye, S., J. P. Canales, R. Rihm, J. J. Dañobeitia, and J. Gallart (1999), A crustal transect through the northern and northeastern part of the volcanic edifice of Gran Canaria, Canary Islands, *J. Geodyn.*, *28*, 3–26.

Zelt, C. A., and P. J. Barton (1998), Three-dimensional seismic refraction tomography: A comparison of two methods applied to data from the Faeroe Basin, *J. Geophys. Res.*, *103*, 7187–7210.

Zelt, C. A., K. Sain, J. V. Naumenko, and D. S. Sawyer (2003), Assessment of crustal velocity models using seismic refraction and reflection tomography, *Geophys. J. Int.*, *153*, 609–626.

Zhao, D., F. Ochi, A. Hasegawa, and A. Yamamoto (2000), Evidence for the location and cause of large crustal earthquakes in Japan, *J. Geophys. Res.*, *105*, 13,579–13,594.

E. R. Flueh, D. Klaeschen, H. Kopp, and C. Papenberg, IFM-GEOMAR, Leibniz-Institute for Marine Sciences, Wischhofstr. 1–3, D-24148 Kiel, Germany. (eflueh@geomar.de; dklaeschen@geomar.de; hkopp@geomar.de; cpapenberg@geomar.de)